AN ABSTRACT OF THE THESIS OF

Ronald Ernest Johnson (name) for the M.S. (degree) in Civil Engineering (major)

Date thesis is presented May 15, 1963.

Title PRESSURE DISTRIBUTION AROUND A CIRCULAR CYLINDER RESTING ON A FLAT BOUNDARY IN AN OSCILLATING FLUID.

Abstract approved [redacted].

This study was undertaken to provide information needed in the design of ocean outfalls.

A review of past investigations concerning forces on submerged objects is presented. Objects independent of any boundary and cylinders in boundary contact are considered.

A solution for pressure distribution about a circular cylinder resting on a flat boundary in an oscillatory fluid is derived. The energy equation is used as a framework for this derivation. The G. B. Airy (1845) equations of particle motion in waves are used with potential flow theories. The resulting pressure distribution equation considers differences in water level with the passing wave and differences in orbital motion of the water particles referenced to depth above the boundary. This pressure distribution equation does not include viscous or inertial effects on the cylinder.

The derived pressure distribution equation is programmed for digital computer solution.

Dimensionless ratios between the measured horizontal force on the cylinder and wave characteristics are organized. Correlation between these dimensionless ratios indicates an increase of force with an increase in wave height for any given depth, although data scatter is present.

The pressure distribution equation is integrated graphically and the resulting net force differs from the corresponding experimental force by 16 percent to 70 percent.

PRESSURE DISTRIBUTION AROUND A CIRCULAR CYLINDER RESTING ON A FLAT BOUNDARY IN AN OSCILLATING FLUID

by

Ronald Ernest Johnson

A thesis

submitted to

OREGON STATE UNIVERSITY

in partial fulfillment of
the requirements for the
degree of

MASTER OF SCIENCE

June 1963

APPROVED:

[redacted]

Assistant Professor of Civil Engineering,
In Charge of Major

[redacted]

Head of Department of Civil Engineering

[redacted]

Dean of Graduate School

Date thesis is presented May 15, 1963

Typed by Betty Thornton

ACKNOWLEDGMENT

Thanks is extended to the Public Health Service for its grant, which made this investigation possible.

Appreciation is extended to Dr. Larry Slotta for his advice and assistance in the preparation of this study and to Jayne Tichenor and Phyllis Van Zyl for their assistance in data processing and manuscript preparation.

The writer wishes to give special acknowledgment to his fiancé, Patricia Sweet, for the many hours assisting in the data collection, processing, and manuscript proofreading.

TABLE OF CONTENTS

LIST OF FIGURES

LIST OF TABLES

LIST OF PHOTOGRAPHS

NOTATION

a = Radius of cylinder.

c = Velocity of wave propagation.

d = Depth of fluid at rest.

H = Wave height.

L = Wave length.

P_o = Pressure in a region of undisturbed fluid.

P = Pressure on the cylinder.

q = Speed of fluid in the Z-plane.

r = Radial distance measured from origin of cylinder.

SWS = Still water surface.

T = Wave period.

t = Fraction of T, in seconds.

U = Potential flow velocity $\equiv V_o$.

u_x = Horizontal component of orbital velocity.

v = Velocity on the cylinder.

V_o = Velocity in a region of undisturbed fluid.

v_y = Vertical component of orbital velocity.

W = Horizontal flow transformation plane.

dw/dz = Complex velocity in the Z-plane.

$d\overline{w}/d\overline{z}$ = Conjugate of the complex velocity.

x = Horizontal coordinate of the cylinder and of the wave.

y = Vertical coordinate of the wave surface.

Yc = Vertical coordinate of the cylinder.

Z = Real plane of flow past the cylinder.

zy = Vertical distance from SWS to the point where the orbital velocity is being determined.

γ = Specific weight of the fluid.

ζ = Transformation plane due to Schwarz-Christoffel.

ρ = Density of the fluid.

PRESSURE DISTRIBUTION AROUND A CIRCULAR CYLINDER RESTING ON A FLAT BOUNDARY IN AN OSCILLATING FLUID

INTRODUCTION

The problem of sewage disposal has confronted society since man started living in communities. A few methods of sewage treatment in use today are removal of treated and untreated effluent by rivers, disposal by deposition in fields, and removal by ocean outfall.

The method of disposal by ocean outfall is currently receiving increased attention, even though this form of disposal has been used for over one hundred years. Large coastal cities are turning to this method of disposal from the other two methods mentioned above. The Los Angeles, California, sludge outfall extends seven miles from shore. Lines can and are being laid out to depths and distances which prevent possible contaminent return to the surf area. Using modern techniques and materials, the outfall pipes can be laid at costs much less than for comparable treatment plants and with insignificant operating costs (5, p. 1453).

Considerable research done in the field of ocean outfall disposal has been concerned with the dilution and stratification of effluent in the open ocean. Recently, W. L. Ryan (17, 1962) conducted research on the dilution of the sewage in transit through the outfall. Little work has been undertaken on the wave characteristics which influence outfall design.

The purpose of this investigation is to determine the pressure distribution around circular cylinders resting on flat boundaries in oscillatory fluid. Dimensionless relationships are to be organized between the force on the cylinder and the wave characteristics.

REVIEW OF PAST INVESTIGATIONS

Test Objects Independent of Boundary Geometry

Early work on the motion of solid bodies through viscous fluids was undertaken by G. G. Stokes (21) and Lord Rayleigh (15, p. 706). Rayleigh determined an equation for the force necessary to maintain an infinite circular cylinder in motion with unit velocity. Rayleigh concluded that the cylinder was much less amenable to mathematical treatment than Stoke's sphere problem. Rayleigh determined the force on the cylinder as:

$$F = \frac{-8\nu M'}{a^2 \log(4\nu t/a^2)} . \qquad (1)$$

The force F is inversely dependent upon the common logarithm of time. This indicates that the force needed to maintain the cylinder in unit velocity motion decreases slowly with increasing time. In Equation (1),

M^1 = Displaced mass of fluid,

a = Cylinder radius,

and t = Time since motion began.

Most of the present day investigators are concerned with finite velocities and accelerations. The resistance to the accelerating movement of objects in a fluid is normally evaluated with an increased mass term known as the "virtual mass." This virtual mass is the mass of the object plus the added mass caused by the motion of the surrounding fluid. The added mass depends on the size, shape,

orientation, and movement of the body through the fluid. The added mass is also affected by the fluid's density and viscosity.

The fluid's inertial effect is that of increasing the mass of the body from M to (M + M'). The term M' is the added mass and (M + M') the virtual mass. Stelson (20, p. 520) said, "The virtual mass is the inertia coefficient or ratio of applied force to acceleration in fluid media. The actual mass of a body is the inertia coefficient that applies to movement in a vacuum." The virtual mass will be only slightly greater in air than in a vacuum, but it will be of considerable importance in a fluid. Whenever submersed objects are accelerated, virtual mass is a factor that should not be overlooked. For the case of a cylinder accelerated in water (long axis normal to acceleration), the measured added mass obtained by Stelson (20, p. 524) agrees well with that obtained from potential flow analysis. Theory shows that the mass of the displaced fluid is equal to the mass of the cylinder. The experimental results show that the value of the added mass approaches the mass of the cylinder as the ratio of cylinder length to diameter becomes large ($L/D \longrightarrow \infty$).

However, some experimental results showed that the added mass effect could not be described by a constant value, but is dependent upon the state of motion (8, p. 324). Iversen and Balent (8) have shown that the resistance equation for objects moving in accelerated unidirectional motion is of the same form as that used for steady state motion, that is

$$F = C\rho\frac{V^2}{2}S, \qquad (2)$$

where

$\overline{F}$ = Net fluid resistance,

V = Velocity,

and s = Projected area of test object.

In the case of steady flow, c is equivalent to C_D, the coefficient of drag. In the case of accelerated motion,

$$C = \phi(N_R, N_F, \text{geometry}, AL/V^2), \tag{3}$$

where

N_R = Reynolds number,

N_F = Froude number,

L = Characteristic length of test object, and

AL/V^2 = Correlating modulus.

The term AL/V^2 was shown to be a correlating modulus for accelerated flow, for it contains both an acceleration, A, and velocity, V.

Iversen and Balent performed their investigations using disks accelerated vertically in water. They found that the Froude number did not influence the resistance coefficient. At the onset of motion, Iversen and Balent found that the Reynold's number affected the resistance coefficient.

Values of the added mass factor were evaluated from the data by Iversen and Balent and plotted against the modulus AD/V^2, D being the test disk diameter. The resulting correlation indicated that as the velocity increased the added mass factor increased. Use of a constant added mass factor may be considerably in error in evaluating accelerated

motion, when used with drag coefficients which correspond to steady state values of the velocities.

Other investigators have used Equations (2) and (3) in the investigation of the resistance coefficient, c. Varying results have been obtained. Crooke (6, p. 16) experimented with spheres and cylinders, both horizontal and vertical, obtaining good correlation between the resistance coefficient and the modulus AD/V^2. Both A. D. K. Laird (11) and S. R. Keim (9) investigated cylinders in accelerated motion.

Keulegan and Carpenter (10) and J. S. McNown (12) considered the unsteadiness of flow affecting the total resistance of a submerged body. They combined the steady state drag equation with a pressure gradient term, required to accelerate the ambient flow, and an inertial term, due to additional accelerations throughout the fluid, to give

$$\frac{F}{L} = C_D \rho D \frac{V^2}{2} + \oint (p ds)_x + A_o \rho \frac{d}{dt}(kV).$$

The force caused by the ambient pressure gradient is simply the product of the displaced mass and the ambient acceleration (13, p. 125):

$$F_p = \oint L (p ds)_x = \rho A_o L \frac{dv}{dt}.$$

Thus, the resistance can be expressed as

$$\frac{F}{L} = C_D D \rho \frac{V^2}{2} + A_o \rho \left[\frac{dv}{dt} + \frac{d}{dt}(kV) \right], \qquad (4)$$

where

F/L = Resistance per unit length of cylinder,

L = Cylinder length,

D = Cylinder diameter,

$A_o = \pi D^2/4$, the cross-sectional area of the cylinder,

and K = Virtual mass coefficient.

Keulegan and Carpenter proceeded further to consolidate Equation (4) by introducing two new coefficients, K' and C_m, such that

$$K'\frac{dv}{dt} = \frac{d}{dt}(Kv)$$

and defining

$$C_m = (K'+1).$$

Equation (4) becomes (10, p. 423)

$$\frac{F}{L} = C_m \rho A_o \frac{dv}{dt} + C_D D \rho \frac{v^2}{2}. \qquad (5)$$

From Equation (5), Keulegan and Carpenter investigated the coefficients C_m and C_D of cylinders and plates in simple sinusoidal currents. They found that the average values of the inertia coefficient, C_m, and drag coefficient, C_D, showed variations over a wave cycle when the intensity of the current and the size of the test objects were changed.

A correlation was made with the period parameter U_mT/D, where

U_m = Maximum intensity of the sinusoidal current,

T = Wave period,

and D = Cylinder diameter or plate width.

For the cylinders, $U_mT/D = 15$ is a critical condition, yielding the

lowest value of the inertia coefficient and the largest value of the drag coefficient (10, p. 434-435).

Difficulty arises when an attempt is made to solve Equation (5) analytically. Both the coefficient of drag, C_D, and the coefficient of virtual mass, k, (incorporated in C_m) depend on the period and are functions of time. A later paper, presented jointly by McNown and Keulegan (13), gave evidence of a unique relationship between C_D and k for both plates and circular cylinders. Equation (5) could be solved numerically with such a relationship known. McNown and Keulegan gave no evidence of a solution having been obtained.

Test Objects in Contact with Boundary Geometry

Harlemann and Dean (7, p. H.1 - H.14) have used the approach of Equation (5) to conduct tests on the forces exerted on a vertical cylinder by wave motion. Equation (5), in differential form, was integrated along the length of a vertical pile, from the bottom to the still water surface. The G. B. Airy equations [1/] for particle velocities and accelerations were used in the integration, with the following dimensionless equation resulting for the total horizontal force:

$$\frac{F}{\rho D^3} = \frac{\pi}{8}\frac{H}{D} C_m \tanh(kh)\cos\theta + \frac{C_D}{4}\left(\frac{H}{D}\right)^2 \frac{kh}{\sinh 2kh}\left[\frac{1}{2} + \frac{\sinh(2kh)}{4kh}\right] \left[|\sin\theta|\sin\theta\right], \quad (6)$$

where H = Wave height,

h = still water surface depth,

1/ See page 21 for specific reference.

D = Pile diameter,

θ = Wave phase angle, varies from zero to 360^{o},

k = Wave number, $2\pi/L$,

and L = Wave length.

Harlemann and Dean determined that the maximum force on the vertical pile occurred at some phase angle between zero and 90^{o}.

Harlemann and Dean approximated the coefficients C_m and C_D by mean values of 2.0 and 0.5 respectively, although there was considerable data scatter.

Beckmann and Thibodeaux (4, p. 130) state that:

> Two phenomena are experienced in the oscillating flow around bodies attached to flat walls: (1) The wall itself has a "streamlining" effect on the flow and thereby reduces the drag coefficient of a blunt body to approximately two-thirds of that of the same configuration without the plate situated along the line of symmetry; and (2) the oscillatory motion permits only fully developed turbulent flow configurations. The resulting drag coefficients correspond to those experienced at super-critical Reynold's numbers.

Thus, for a smooth cylinder resting on a flat boundary, the drag coefficient range may be expected between $0.35 \leq C_D \leq 0.40$. Beckmann and Thibodeaux also approached the subject of lift of a pipe in contact with a boundary and found that values of the lift coefficient C_L varied between $0.34 \leq C_L \leq 0.65$. Their conclusions were: "Circular pipes attached to the ground develop lift forces in flowing media that are similar in magnitude to the drag forces that are experienced" (4, p. 135).

I. Alterman (3, p. 149) questioned the validity of the simplification in determining the drag and lift coefficients used by Beckmann

and Thibodeaux. Alterman indicated that to find the "....wave force coefficients for submarine pipelines would require a voluminous book using standard methods."

However, Alterman (2, p. 32) presented a formula for the resistance, R, of pipe of unit length to wave action as

$$R = \frac{4\pi^2 g \rho b^4}{f^2 e^2} \tag{7}$$

where b = Cylinder radius,

f = Water depth (to still water surface),

and e = Naperian constant, 2.71828+.

This formula requires that the cylinder be placed horizontally on the bottom and normal to the direction of wave propagation. It is seen, according the Equation (7), that the resistance changes as the fourth power of the pipe radius and inversely as the square of the water depth. Further, Equation (7) holds only for deep water theory ($f \gg b$).

Summary

Most of the investigations reviewed primarily centered on the determination of C_m and C_D when the test objects were accelerated. Most accelerations considered were linear. A simplifying condition was that the test objects were generally independent of any boundary.

The pressure distribution equation derived in the next section and the experimental results obtained will primarily be functions of the wave characteristics, a condition not considered by the investigators mentioned previously.

ANALYSIS

Analytical Analysis for Pressure Distribution

Introduction. The previous section has outlined many investigations concerning the special case of flow past an object independent of any boundary geometry. One of the purposes of this paper is to investigate analytically the pressure distribution around a circular cylinder in contact with a boundary and submerged in unsteady fluid motion. It is felt that this development, as well as the experimental force data obtained, will be of use in later work on the derivation of the forces acting on the cylinder.

The energy equation is used as a framework in the following analysis. Potential flow theories are introduced as well as the Airy (1) equations of particle motion in waves. The resulting equation considers differences in water level with the passing wave and differences in orbital motion of the water particles referenced to depth above the boundary, but it does not include viscous or inertial effects on the cylinder.

Steady Flow Solution. Considering the pattern of flow for only the horizontal plane, the energy (Bernoulli) equation can be written in terms of pressure and velocity as

$$\rho\frac{V^2}{2} + P = \rho\frac{V_o^2}{2} + P_o . \tag{8}$$

Rearranging the terms and simplifying gives

$$P = P_0 + \frac{\rho}{2}(V_0^2 - V^2)$$
$$= P_0 + \rho\frac{V_0^2}{2}\left[1 - \left(\frac{V}{V_0}\right)^2\right], \tag{9}$$

where P_0 and V_0 are the respective pressure and velocity of undisturbed fluid motion. ρ is the ambient flow density. P and V are the respective pressure and velocity on the cylinder. Equation (9) provides the vehicle for both the steady flow and oscillating flow pressure distribution equations.

A complex potential flow equation is developed by Milne-Thomson (14, p. 171-175) for flow over a mound resting on a flat boundary. (See Figure 1). The transformation equations are

$$W = U2ci\cot\frac{\zeta}{n} \tag{10}$$

and

$$Z = ic\cot\frac{\zeta}{2}. \tag{11}$$

Z represents a two-dimensional plane with flow past the mound, while W is a plane representing horizontal flow with no boundary effects. The free stream velocity is represented by U, while c is the distance OB = OA in Figure 1. n is a real constant and ζ (zeta) is the transformation plane of the Schwarz-Christoffel theorem (22, Chapter 6). When n equals unity, a semicircular mound is obtained and the flow pattern represents the top half of the flow about a circular cylinder in free space (19, p. 237-246; 18, p. 221-229; 14, p. 154-155; 22, p. 120-126).

For the flow past a cylinder on a flat boundary, the points A and

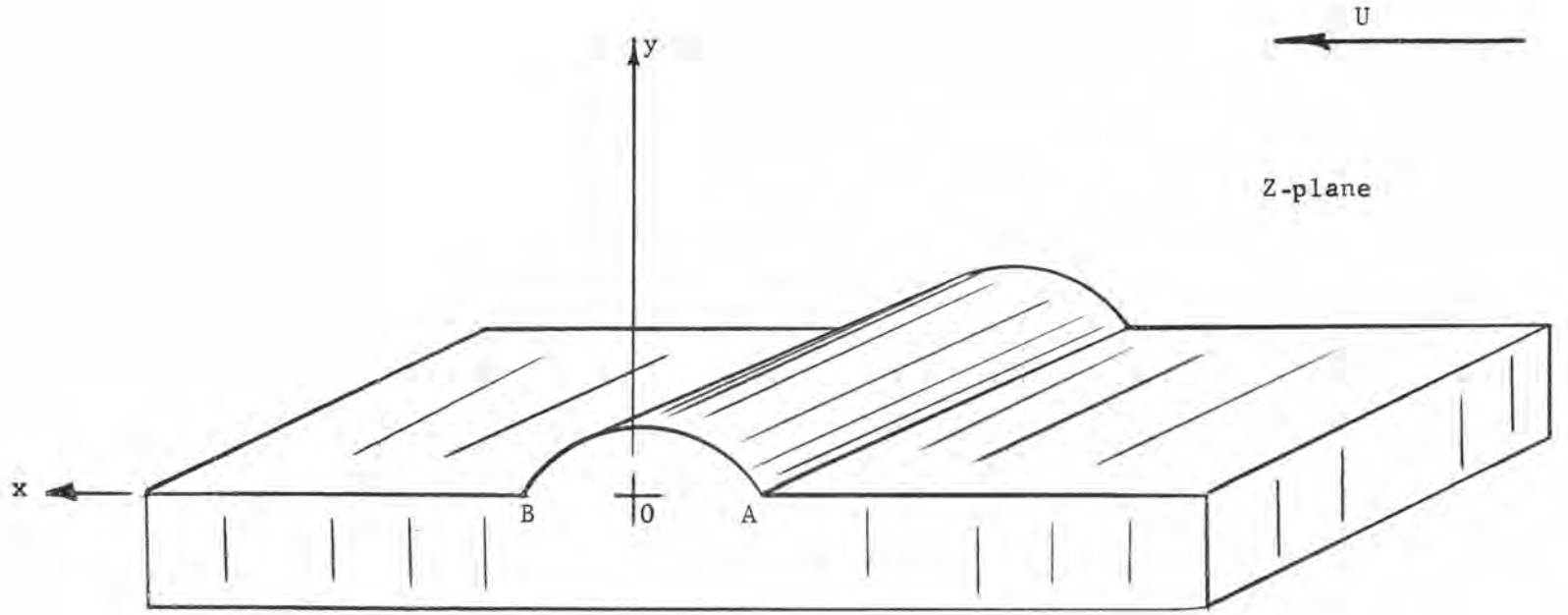

Figure 1. Potential flow past a mound. Complex flow in the Z-plane.

B in Figure 1 are brought into coincidence. The radius of the cylinder, a, formed is

$$a = \frac{c}{\sin\left(\frac{n\pi}{2}\right)} . \tag{12}$$

As A → B, C → zero and, therefore, n → zero from Equation (12) and $\zeta \rightarrow$ zero from Equation (11). Thus, when c is very small, Equations (12) and (11) give

$$a = \frac{2c}{n\pi} \tag{13}$$

and

$$z = \frac{2ic}{\zeta} . \tag{14}$$

Substitution into Equation (10) gives the W-plane potential as

$$\begin{aligned} W &= ia\pi U \cot\left(\frac{ia\pi}{z}\right) \\ &= a\pi U \coth\left(\frac{a\pi}{z}\right) \end{aligned} \tag{15}$$

Equation (15) is the complex potential of the flow past a circular cylinder of radius a, free stream velocity U, resting on a flat boundary (See Figure 2).

The speed squared in the Z-plane is equal to

$$q^2 = \left(\frac{dw}{dz}\right)\left(\frac{d\bar{w}}{d\bar{z}}\right),$$

where dw/dz is the complex velocity in the Z-plane and $d\bar{w}/d\bar{z}$ is the conjugate of the complex velocity in the Z-plane. Differentiation and substitution gives

$$q^2 = \frac{a^4\pi^4U^2}{r^4}\left(\frac{2}{\cosh\left(\frac{2a\pi x}{r^2}\right) - \cos\left(\frac{2a\pi y}{r^2}\right)}\right)^2 \tag{16}$$

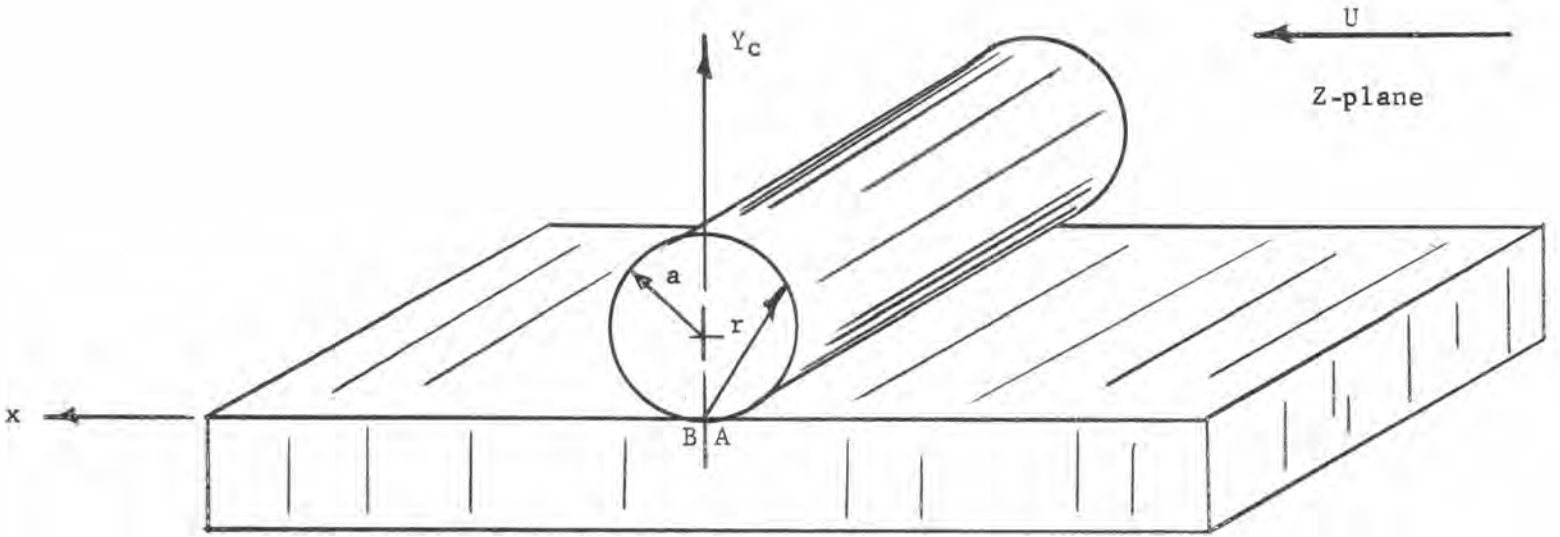

Figure 2. Potential flow past a cylinder on a flat boundary, Z-plane.

after rearranging and simplifying. On the cylinder

$$r^2 = 2a y_c. \tag{17}$$

Substitution of Equation (17) into Equation (16) gives

$$q_t^2 = \frac{a^2\pi^4 U^2}{4(y_c)^2}\left(\frac{2}{1+\cosh\left(\frac{2a\pi x}{r^2}\right)}\right)^2 = \frac{a^2\pi^4 U^2}{4(y_c)^2\cosh^4\left(\frac{a\pi x}{r^2}\right)}. \tag{18}$$

The speed (Equation (18)) is considered positive when flow is from right to left. Y_c and x are the coordinates of the rim of the cylinder, and r is a chord length measured from the origin of the cylinder as shown in Figure 2.

The speed, q_t, on the cylinder can be substituted into Equation (9). This assumed potential flow gives possible velocities on the cylinder. In reality, the flow on the surface of any structure is zero. Upon substitution, the pressure distribution equation gives

$$P = P_0 + \rho\frac{V_0^2}{2}\left[1 - \left(\frac{\frac{a^2\pi^2 U}{2(y_c)^2\cosh^2(a\pi x/r^2)}}{V_0}\right)^2\right].$$

The velocity V_0, in this case, equals identically the free stream velocity U. Hence,

$$P = P_0 + \rho\frac{U^2}{2}\left[1 - \frac{a^2\pi^4}{4(y_c)^2\cosh^4(a\pi x/r^2)}\right]. \tag{19}$$

Equation (19) yields the pressure distribution around a circular cylinder resting on a flat boundary in steady flow, as both P_0 and U

are constant.[2/] As can be seen in Figure 3, a symmetrical pressure distribution about a vertical axis results from Equation (19). The bottom of the cylinder has the greatest pressure, always positive, while the pressure on the top of the cylinder can be negative if the velocity over the cylinder is great enough or the ambient pressure, P_o, small enough. Table 6 and Figure 12 in Appendix II show selected points on the theoretical distribution of pressure for the steady flow case, for comparison with the oscillating flow case.

Oscillating Flow Solution. Because the water movement in the ocean is of oscillatory nature, rather than steady motion, Equation (19) should be modified. The pressure term, P_o, is varient with either time or distance or both (assuming a level bottom). Wave motion in the open ocean is called "sea" and is generally a combination of several different wave patterns. When each wave train is taken independently at considerable distance from the point of propagation, it becomes a swell which approaches sinusoidal motion. Swell conforms very nearly to the theoretical equations and this sinusoidal condition will be assumed in further discussion of the oscillating flow solution.

Thus, P_o, will vary from some still water surface (SWS) hydrostatic pressure to an increased or decreased pressure, depending upon the fluctuating wave condition at the point in question. Milne-Thomson (14, p. 389) presents an approximation for the wave profile as

$$y = a \sin \frac{2\pi}{\lambda}(x - ct),$$

2/ P_o is constant for any given depth. It must be adjusted for different positions on the cylinders. See page 20.

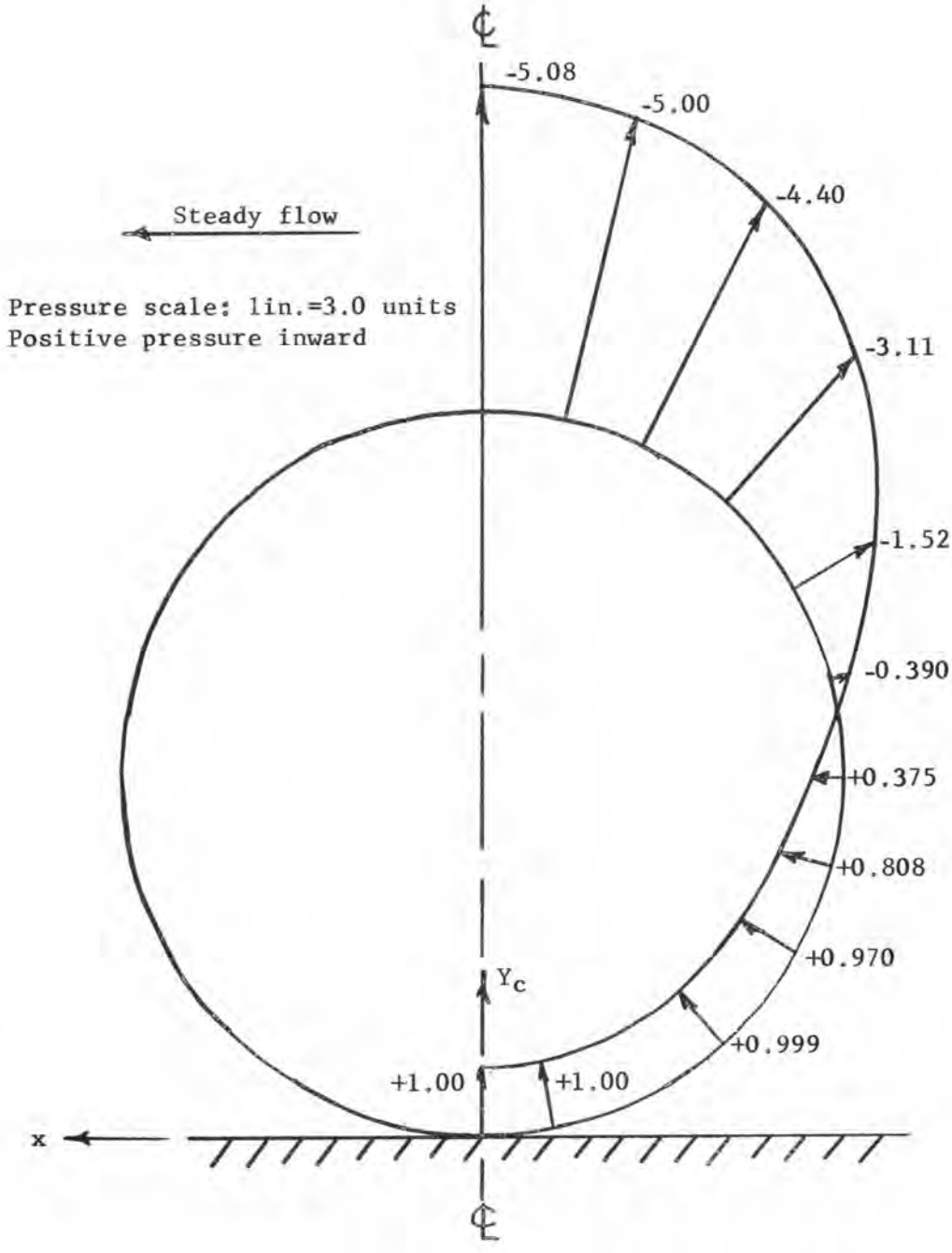

Figure 3. Steady flow pressure distribution about a circular cylinder, assuming $P_o = 0$, $1/2\rho U^2 = 1$.

or

$$y = \frac{H}{2} \sin \frac{2\pi}{L}(x - ct)$$

or

$$y = \frac{H}{2} \sin 2\pi \left(\frac{x}{L} - \frac{c}{L} t\right),$$

where the relationship between the velocity of propagation c and wave length L is

$$L = cT,$$

T being the wave period. The wave profile now becomes

$$y = \frac{H}{2} \sin 2\pi \left(\frac{x}{L} - \frac{t}{T}\right), \tag{20}$$

where y and x are the respective vertical and horizontal coordinates of the water surface and H the wave height. Values of x are measured from a vertical datum through the center of the cylinder. y is measured positively upward from the still water surface (SWS). Figure 4 illustrates the three conditions of t = o, t = 1/4T, and t = 1/2T, with x varied from x = 0 to x = L in the three cases.

P_o consists of the stillwater depth d and the fluctuation due to wave passage, where the fluctuation, y, can be negative as well as positive.

$$P_o = \gamma[d + y]$$

$$= \gamma\left[d + \frac{H}{2} \sin 2\pi \left(\frac{x}{L} - \frac{t}{T}\right)\right]$$

or

$$P_o = \gamma\left[d + \frac{H}{2} \sin\theta\right],$$

where

$$\theta = 2\pi \left(\frac{x}{L} - \frac{t}{T}\right).$$

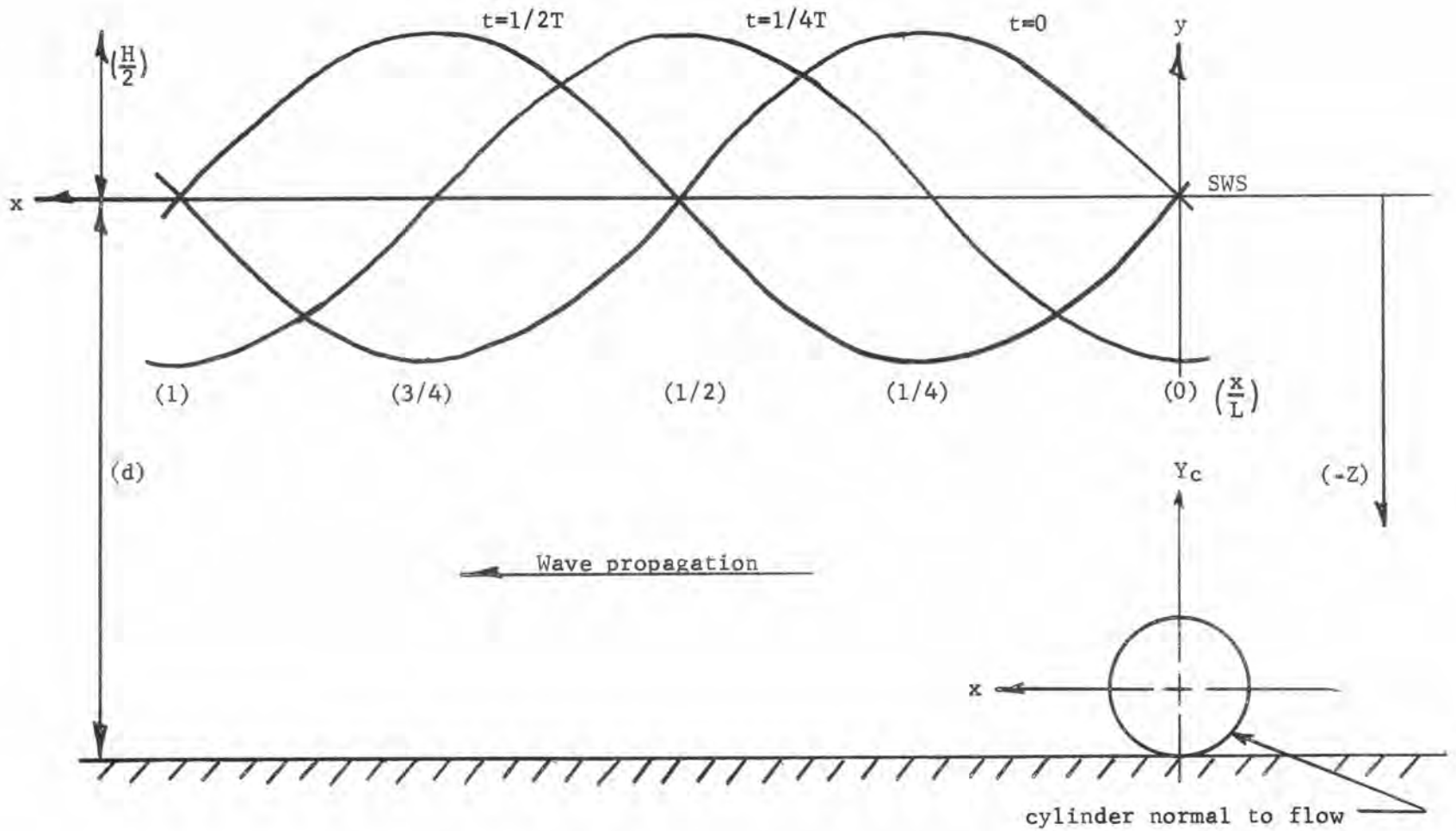

Figure 4. Water surface variation due to sinusoidal motion and time.

This equation gives the pressure on the bottom and does not consider the cylinder coordinate Y_c. Y_c must be subtracted from d to give P_o at the level under consideration. P_o now becomes

$$P_o = \gamma\left[d - y_c + \frac{H}{2}\sin\theta\right]. \tag{21}$$

R. G. Dean and P. S. Eagleson (7, p. H-3) give the above wave profile (Equation (20)) to the second approximation as

$$y = \frac{H}{2}\sin 2\pi\left(\frac{x}{L} - \frac{t}{T}\right) - \left[\frac{\pi H^2}{8L}\cosh(2\pi d/L)(2+\cosh 4\pi d/L)\right] \left[\frac{\cos 4\pi\left(\frac{x}{L} - \frac{t}{T}\right)}{(\sinh 2\pi d/L)^3}\right]. \tag{22}$$

The second part of Equation (22) on the right of the equality gives the second approximation correction term which will be neglected in the present discussion. This wave profile is due to Stokes (21) and actually is an infinite series of terms.

The first term of the Stokes series is the small amplitude wave theory. The successive terms represent correction terms for larger amplitude waves.

Upon substitution into Equation (19), the pressure distribution becomes

$$P = \gamma\left[d - y_c + \frac{H}{2}\sin\theta\right] + \rho\frac{U^2}{2}\left[1 - \frac{a^2\pi^4}{4(y_c)^2\cosh^4(a\pi x/r^2)}\right]. \tag{23}$$

The free stream velocity U can now be taken as the orbital velocity of the fluid particles next to the wall of the cylinder. U varies according to the equations first developed by G. B. Airy (1) as:

$$U_x = \frac{\pi H}{T} \frac{\cosh\left[2\pi(d+z_y)/L\right]}{\sinh(2\pi d/L)} \cos\theta \tag{24}$$

and

$$V_y = \frac{\pi H}{T} \frac{\sinh\left[2\pi(d+z_y)/L\right]}{\sinh(2\pi d/L)} \cos\theta. \tag{25}$$

U_x and V_y are the respective horizontal and vertical components of the orbital velocities. Z_y is the vertical distance from the SWS to the point where the orbital velocity is being determined and is considered positive upward.

The character of the wave is modified as the wave approaches shallow water. Here the depth is less than one-tenth the wave length. Actually, the orbits of the single water particles will be ellipses that flatten to straight, horizontal lines at the bottom. On the boundary, the motion can be only back and forth, and, if the depth is small compared to the wave length, the motion will remain nearly horizontal at all depth. (See Figure 5). This perhaps is due to reflection of the vertical component and could result in increasing the horizontal velocity near the boundary in actual flow situations.

The horizontal component of the orbital velocity will be taken as the total orbital velocity.

$$U \approx U_x = \frac{\pi H}{T} \frac{\cosh\left[2\pi(d+z_y)/L\right]}{\sinh(2\pi d/L)} \cos\theta, \tag{26}$$

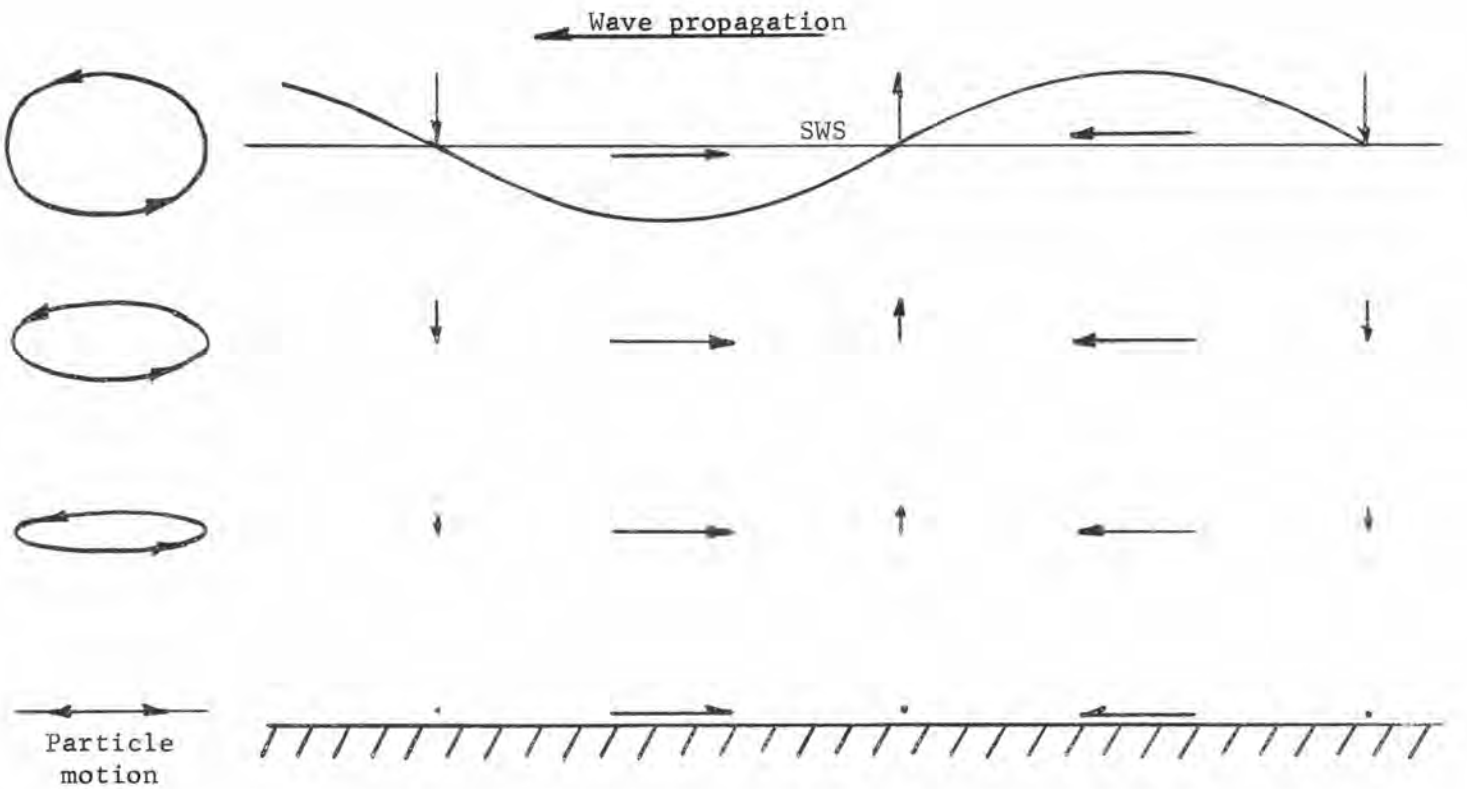

Figure 5. Sketch of idealized orbital motion of a shallow water wave (16, p. 37).

so

$$U^2 = \frac{\pi^2 H^2 \cosh^2\left[2\pi(d+z_y)/L\right]}{T^2 \sinh^2(2\pi d/L)} \cos^2\theta$$

$$= A \cosh^2 B \cos^2\theta$$

where (27)

$$A = \frac{\pi^2 H^2}{T^2 \sinh^2(2\pi d/L)},$$

$$B = 2\pi(d+z_y)/L,$$

and $$\theta = 2\pi\left(\frac{x}{L} - \frac{t}{T}\right).$$

Substituting into Equation (23), the pressure distribution around a circular cylinder on a flat boundary in an oscillatory flow becomes

$$P = \gamma\left[d - y_c + \frac{H}{2}\sin\theta\right] + \left[\rho\frac{A}{2}\cosh^2 B \cos^2\theta\right]$$

$$\left[1 - \frac{a^2\pi^4}{4(y_c)^2 \cosh^4(a\pi x/r^2)}\right]$$

or

$$P = \gamma\left[d - y_c + \frac{H}{2}\sin\theta\right] + \left[A' \cos^2 B \cos^2\theta\right]$$

$$\left[1 - \frac{k}{\cosh^4(\phi)}\right], \qquad (28)$$

where

$$A' = \rho\frac{A}{2},$$

$$\phi = a\pi x/r^2,$$

and $$k = a^2\pi^4/4(y_c)^2.$$

Appendix I contains the flow chart (Figure 11) and solution of Equation (28) for the IBM 1620 FORTRAN computer; Appendix II contains

results for a particular wave at four phases of the wave (quarter points). This can be compared to the steady state solution previously mentioned in Figure 3, and in Appendix II, Figure 12. Graphical integration results are presented in Table 3. In Table 3 the horizontal pressure force obtained by graphical integration is compared to the measured drag.

Dimensional Analysis For Force Measurement.

In the analysis of the force on the cylinder several dimensionless ratios will be determined using the principles of dimensional analysis and Buckingham's pi-theorum. This analysis will provide functional relationships between the dependent variable, force, and the independent variables, wave length, depth, wave height, cylinder diameter, fluid density, gravity, wave velocity, and α , the angle the cylinder makes with the approaching wave.

The dependent variable, force, can mathematically be expressed as

$$F = f\left(L, h, H, D, \rho, g, C, \alpha\right). \tag{29}$$

Several of the above variables are dependent upon each other and can be removed from detailed consideration as follows. In deep water, the velocity of wave propagation is given as

$$C = \left(\frac{gL}{2\pi} \tanh \frac{2\pi h}{L}\right)^{\frac{1}{2}}. \tag{30}$$

Equation (30) indicates that the wave velocity is dependent upon the wave length, depth of water, and gravity. Since velocity is a function

of L, h, and g, it can be neglected in Equation (29).

Due to the nature of the experimental equipment (see page 27), only shallow waves can be generated. These generated waves can be nearly described as shallow solitary waves. The wave velocity for a solitary wave is independent of the wave length and allows the wave length to be dropped from further consideration.

The following equation includes the important remaining variables:

$$F = f'(h, H, D, \rho, g, \alpha). \tag{31}$$

Each of the variables in Equation (31), with the exception of α, has dimensions which can be expressed in terms of either force, length, and/or time (F-L-T). In this case, the pi-theorem will reduce the number of dimensionless parameters from six to three because each of the three fundamental dimensions is involved more than once.

Upon application of the pi-theorem, the following dimensionless ratios were obtained:

$$\frac{h}{D}, \frac{H}{D}, \frac{Fg}{\rho D^5}$$

where D, the cylinder diameter, ρ, and g were selected as repeating variables due to their constant values. Equation (31) now takes the dimensionless form

$$\frac{Fg}{\rho D^5} = f''\left(\frac{h}{D}, \frac{H}{D}, \alpha\right). \tag{32}$$

The independent dimensionless ratios were varied individually to determine the effect upon the force ratio, $F_g/\rho D^5$. For the cases

tested, the angle α was 0^{o} (that is the cylinder was parallel to the approaching wave). The effects of h/D and H/D on $F_g/\rho D^5$ are shown graphically in Figure 9. (See page 35.)

TEST EQUIPMENT AND PROCEDURE

Test Equipment

The experimental tests were conducted in the Engineering School wave tank. The tank is 48 feet long, 18 inches wide, 24 inches high, and consists of eight six-foot glass-walled sections. A pneumatic drive wave generator produces waves which nearly reproduce shallow water particle motion (Figure 5). The waves were fully dissipated so reflected motion and standing waves were eliminated.

The test cylinder was mounted such that it nearly touched the bottom (Photograph 1). The cylinder was allowed to deflect laterally under the influence of the wave. Two rigid 1/2-inch diameter rods transmitted the deflection to four SR-4 strain gages. This system was rigidly attached to the top of the wave tank as shown in Figure 6.

The four strain gages were mounted on the reduced cross section of a thin flexible plastic member (Photograph 2). The deflection due to the waves was then concentrated at the gage location. All four gages were used as active members on the Wheatstone bridge of the Brush Universal Analyzer, which converted the change in strain gage resistance to an electrical impulse. A Brush oscillograph then was used to record the trace of the force exerted by a passing wave.

Plastic tubes were fitted over the support rods and fitted rigidly to the tank walls (Photograph 1). The influence of the support rods was thus reduced in deep water or high waves. Two short cylinder

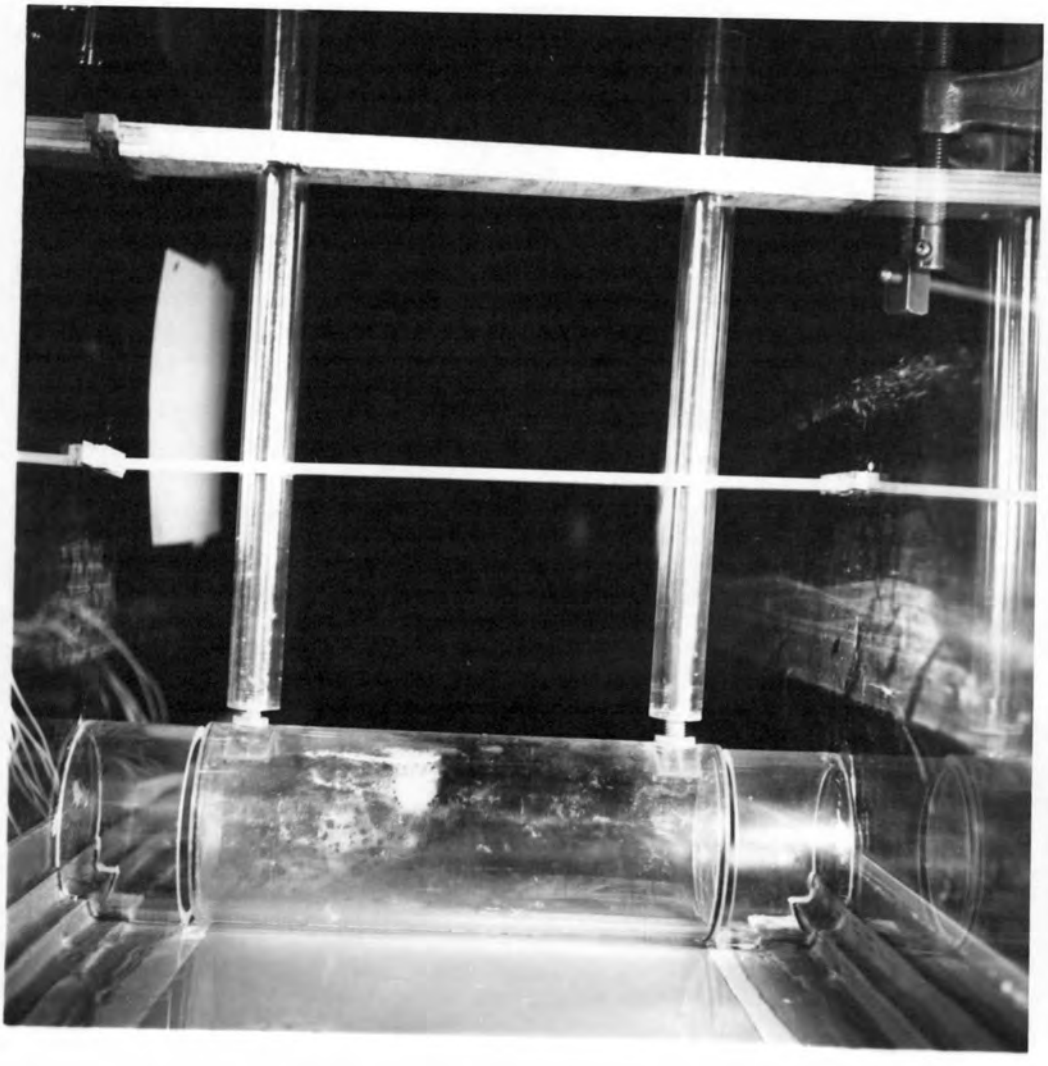

Photograph 1. Test cylinder installation, dry bed.

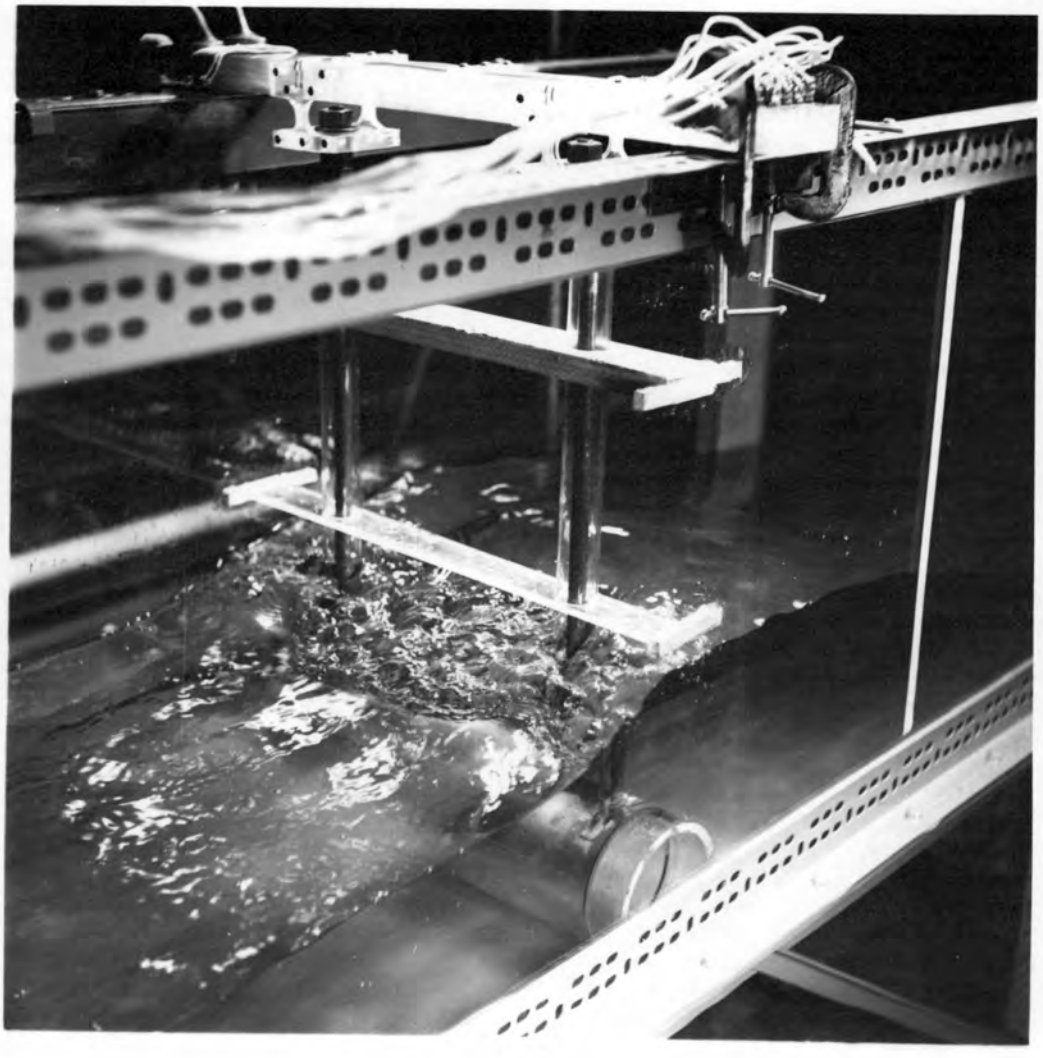

Photograph 2. Test cylinder strain gage mounting detail visible. Still water depth = 8 inches.

Direction of wave propagation from right to left.

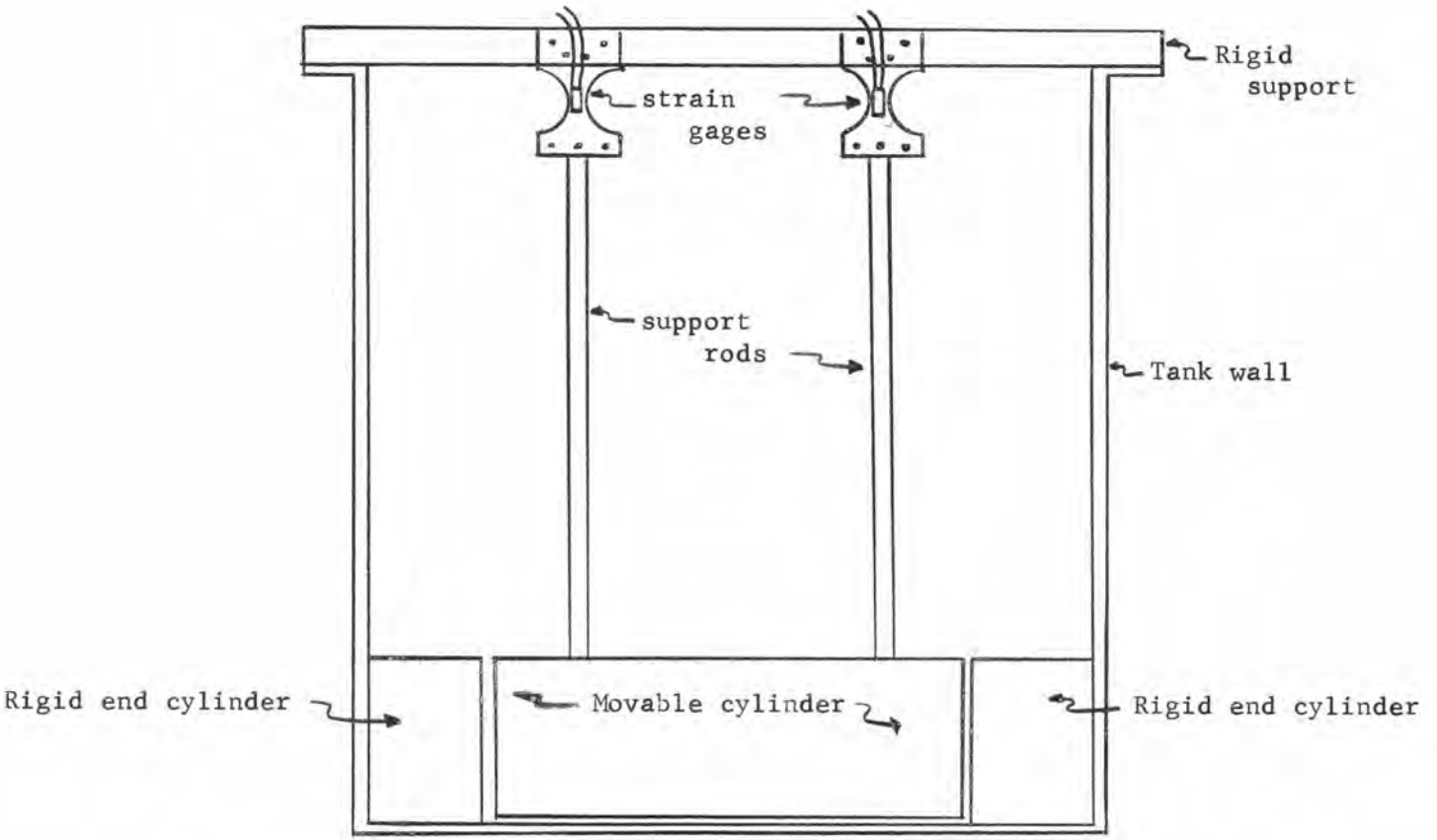

Figure 6. Line drawing of test cylinder suspension system.

segments were cemented to the tank walls to approximate a continuous cylinder (See Figure 6 and Photograph 1).

Procedure

Figure 7 illustrates the method of calibration used to determine the horizontal forces on the test cylinder. Known weights were hung from the pulley system. The resulting deflection on the oscillograph trace indicated the lateral force parallel to the boundary on the cylinder. The calibration curve obtained was linear and is shown in Figure 8.

The variables, wave length, depth of water, and height of wave, were obtained by observation. The period was obtained from the oscillograph. The velocity of the waves was found to compare favorably with the theoretical wave velocity at all depths. The measured velocity for all depths was within seven percent of the theoretical.

With the wave generator running on constant settings, a set of runs was made varying the water depth from three inches to 14 inches. A range of wave lengths and wave heights was obtained with a constant, or nearly constant, wave period. The wave generator setting was then changed for a new run. Each trace was produced at a chart speed of 25 mm per second. The wave period was obtained by measuring the length of the reproduced wave on the chart and dividing by the chart speed. This simple calculation prevented repetition of data, although two sets with a period = 1.86 seconds were taken. These two sets (E and I) were used to check the reproducibility of the wave generator.

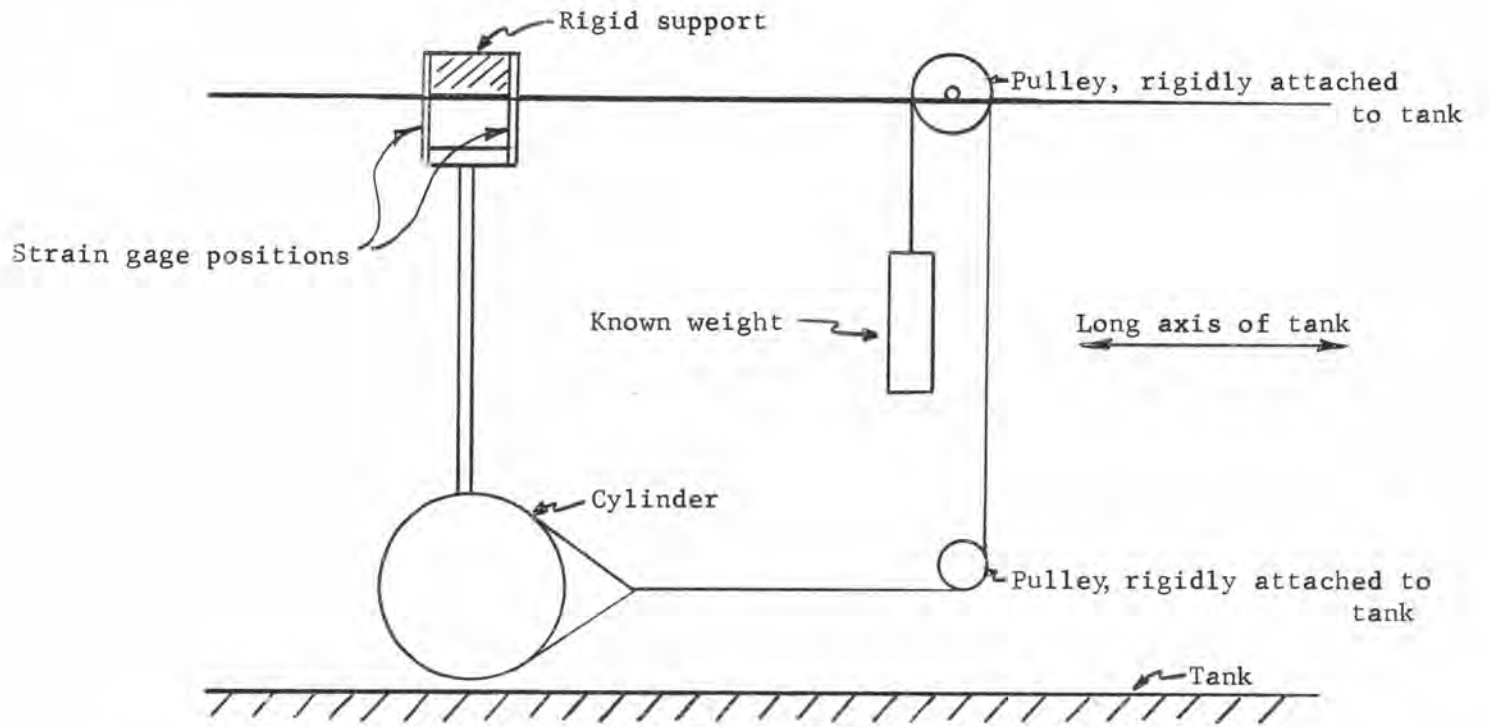

Figure 7. Line drawing of calibration equipment for experimental force measurements.

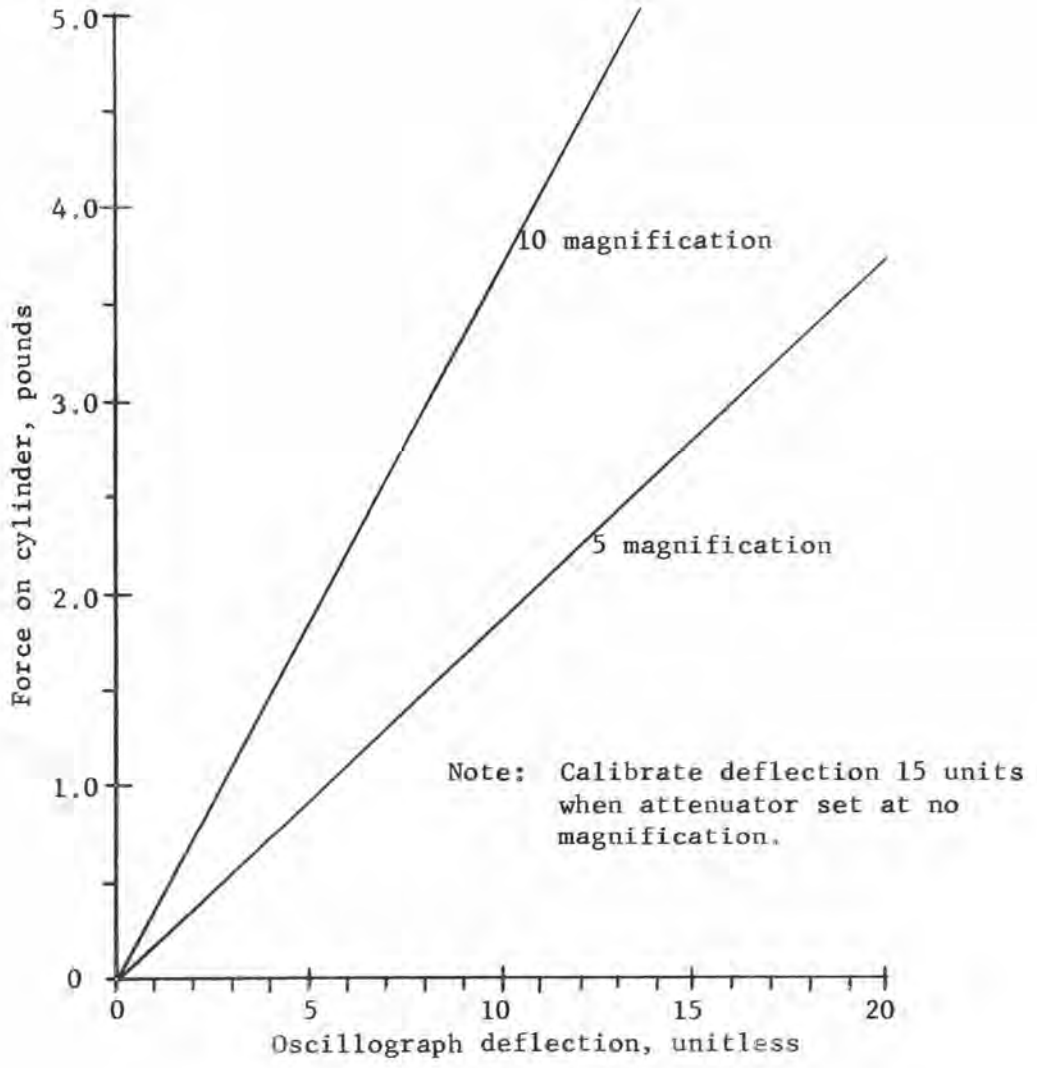

Figure 8. Calibration curve, oscillograph deflection versus force.

EXPERIMENTAL RESULTS

Dimensional Analysis Results

Experience of the first 31 runs indicated that the wave generator should be left running on a constant setting, while varying the water depth. Little correlation was obtained when random generator settings were used with constant depth.

Two separate wave generator settings were used to obtain Runs 32 through 54. The dimensionless ratios obtained, compared to Figure 9, formed a displaced plot of h/D. With protection about the support rods and the cylinder segments in place for similar conditions, correlation is indicated as shown in Figure 9. This showed that the cylinder segments were more important in the actual force determination than the support rod protection.

The exposed support rods tended to increase the measured force with increasing depth. The absence of the cylinder segments allowed particle flow around the test cylinder, which decreased the measured force. The movement of the water particles around the test cylinder was noted using dye traces. The movement was more erratic and turbulent in nature than when the cylinder segments were included to form the continuous cylinder across the wave tank.

The nine data sets used in the final analysis, with rod support protection and end cylinder segments in place, are included in Table1. Figure 9 is the plot of computed dimensionless ratio data listed in Table 2 for the nine sets. Considerable data scatter is evident for

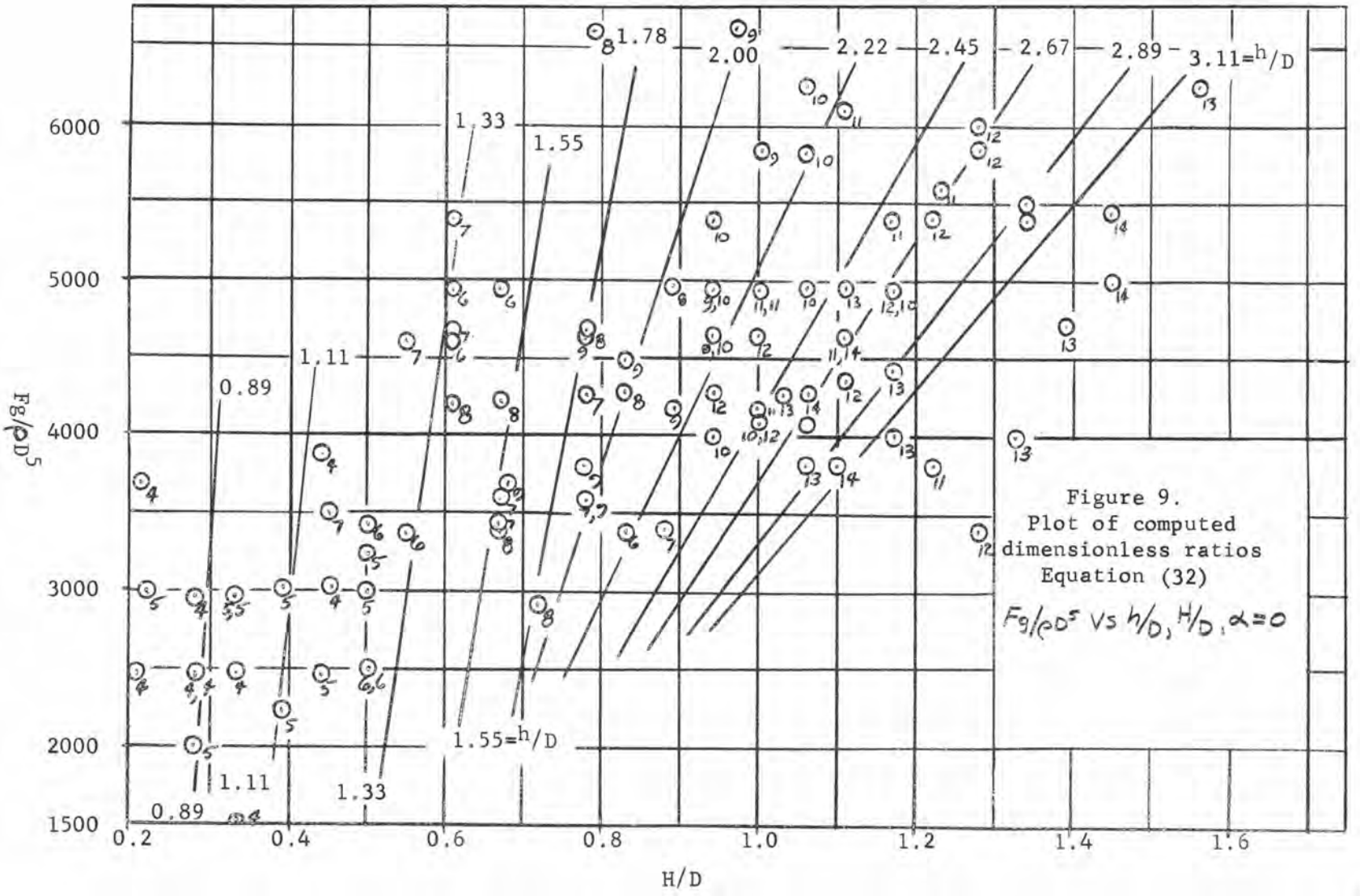

Figure 9.
Plot of computed dimensionless ratios Equation (32)

$F_g/\rho D^5$ vs h/D, H/D, $\alpha = 0$

Table 1. Force and wave characteristic data from Runs 55-164, Sets A-I.

Run	Wave Length ft.	Depth ft.	Wave Height ft.	Period sec	Wave Velocity ft/sec	Force	
						Units	Pounds
A 55	12.00	1.000	0.479	2.18	5.51	8.0	1.5
56	11.67	0.916	0.458	2.18	5.35	9.0	1.7
57	11.25	0.834	0.417	2.16	5.21	12.0	2.2
58	10.67	0.750	0.292	2.16	4.93	9.0	1.7
59	9.92	0.667	0.292	2.14	4.86	11.0	2.1
60	9.42	0.583	0.333	2.12	4.47	8.0	1.5
61	9.17	0.500	0.312	2.10	4.37	8.0	1.5
62	7.42	0.417	0.146	2.10	3.53	5.5	1.0
63	6.75	0.333	0.104	2.10	3.22	6.0	1.1
64	6.50	0.250	0.083	2.10	3.10	7.0	1.3
65	5.00	0.167	0.08	2.23	2.23	1.0	0.15
B 66	3.00	0.167	0.10	1.40	2.14	1.0	0.15
67	3.17	0.250	0.10	1.40	2.26	2.0	0.3
68	4.67	0.333	0.125	1.40	3.33	3.5	0.65
69	5.83	0.417	0.167	1.40	4.17	6.0	1.1
70	6.00	0.500	0.188	1.40	4.29	6.0	1.1
71	6.83	0.583	0.292	1.40	4.89	10.0	1.9
72	7.50	0.667	0.250	1.40	5.31	10.0	1.9
73	7.75	0.750	0.375	1.44	5.38	14.0	2.6
74	7.67	0.834	0.396	1.44	5.33	14.0	2.6
75	8.33	0.916	0.354	1.52	5.48	12.0	2.2
76	8.42	1.000	0.354	1.48	5.69	10.0	1.9
77	9.00	1.083	0.396	1.52	5.92	9.0	1.7
78	9.58	1.167	0.417	1.52	6.30	9.0	1.7
C 79	9.92	1.167	0.396	1.78	5.58	10.0	1.9
80	9.83	1.083	0.396	1.76	5.65	10.0	1.9
81	9.75	1.000	0.437	1.72	5.66	10.0	2.2
82	9.50	0.916	0.437	1.74	5.46	13.0	2.4
83	9.00	0.834	0.354	1.74	5.17	12.0	2.2
84	8.42	0.750	0.354	1.72	4.89	12.0	2.2
85	8.00	0.667	0.333	1.72	4.65	11.0	2.1
86	7.33	0.583	0.292	1.70	4.31	8.5	1.6
87	6.50	0.500	0.188	1.70	3.82	6.0	1.1
88	5.50	0.417	0.100	1.72	3.20	5.0	0.9
89	5.08	0.333	0.125	1.70	2.99	6.0	1.1
90	4.83	0.250	0.10	1.70	2.84	6.0	1.1
91	3.67	0.167	0.10	1.68	2.19	2.2	0.4

Table 1. Force and wave characteristic data from Runs 55-164, Sets A-I (Continued)

Run	Wave Length ft.	Depth ft.	Wave Height ft.	Period sec	Wave Velocity ft/sec	Force	
						Units	Pounds
D 92	5.75	0.250	0.06	2.08	2.76	8.3	1.57
93	6.33	0.333	0.08	2.08	3.04	8.8	1.65
94	6.83	0.417	0.125	2.12	3.22	7.0	1.32
95	7.78	0.500	0.208	2.12	3.67	8.0	1.50
96	9.05	0.583	0.208	2.12	4.26	11.0	2.05
97	9.92	0.667	0.354	2.12	4.68	11.0	2.07
98	10.50	0.750	0.333	2.15	4.88	10.0	1.87
99	11.63	0.834	0.396	2.16	5.38	12.2	2.22
100	11.92	0.916	0.500	2.14	5.56	13.5	2.50
101	11.67	1.000	0.479	2.14	5.45	14.0	2.60
102	11.67	1.083	0.521	2.14	5.44	11.2	2.10
103	12.08	1.167	0.500	2.15	5.62	13.0	2.40
E104	11.75	1.167	0.542	1.90	6.18	12.2	2.22
105	10.75	1.083	0.437	1.90	5.66	9.6	1.80
106	10.29	1.000	0.417	1.88	5.48	10.5	1.95
107	9.46	0.917	0.396	1.88	5.03	9.8	1.83
108	9.08	0.834	0.375	1.88	4.83	9.8	1.83
109	8.25	0.750	0.292	1.86	4.44	8.6	1.61
110	7.50	0.667	0.271	1.88	3.99	7.0	1.30
111	6.96	0.583	0.250	1.84	3.79	8.1	1.52
112	6.83	0.500	0.229	1.84	3.71	12.0	2.20
113	6.25	0.417	0.188	1.84	3.40	7.7	1.45
114	5.42	0.333	0.167	1.84	2.95	7.2	1.35
115	4.92	0.250	0.125	1.82	2.71	5.3	1.00
F116	3.58	0.167	0.06	1.5	2.39	2.5	0.45
117	4.25	0.250	0.08	1.50	2.84	6.5	1.20
118	4.42	0.333	0.10	1.50	2.95	7.0	1.32
119	4.50	0.417	0.188	1.50	3.00	7.0	1.32
120	5.50	0.500	0.208	1.50	3.67	10.0	1.87
121	6.50	0.583	0.229	1.48	4.39	13.0	2.40
122	7.08	0.667	0.292	1.48	4.78	16.0	2.93
123	7.50	0.750	0.375	1.46	5.14	17.0	3.14
124	7.63	0.834	0.396	1.48	5.16	15.0	2.78
125	7.83	0.917	0.416	1.50	5.22	14.5	2.70
126	8.67	1.000	0.458	1.54	5.64	13.0	2.40
127	8.92	1.083	0.417	1.54	5.79	12.0	2.20
128	9.58	1.167	0.417	1.54	6.22	11.0	2.07

Table 1. Force and wave characteristic data from Runs 55-164, Sets A-I (Continued)

Run	Wave Length ft.	Depth ft.	Wave Height ft.	Period sec	Wave Velocity ft/sec	Force	
						Units	Pounds
G129	8.00	1.167	0.771	1.38	5.80	15.0	2.78
130	7.33	1.083	0.500	1.34	5.48	9.5	1.80
131	6.92	1.000	0.375	1.32	5.24	10.0	1.87
132	6.00	0.916	0.375	1.30	4.62	12.0	2.20
133	5.71	0.834	0.354	1.28	4.17	13.0	2.40
134	5.33	0.750	0.312	1.28	4.17	10.75	2.00
135	5.33	0.667	0.312	1.30	4.07	10.2	1.90
136	5.17	0.583	0.229	1.26	4.11	11.0	2.07
137	4.92	0.500	0.188	1.26	3.91	8.0	1.52
138	4.00	0.417	0.083	1.26	3.18	7.0	1.32
139	3.33	0.333	0.063	1.20	2.98	6.0	1.11
140	3.17	0.250	0.063	1.23	2.58	4.5	0.85
H141	5.50	0.250	0.063	1.92	2.86	7.0	1.32
142	5.83	0.333	0.104	1.92	3.04	6.0	1.11
143	6.42	0.417	0.125	1.96	3.27	7.0	1.32
144	6.88	0.500	0.125	1.96	3.51	11.0	2.05
145	8.08	0.583	0.167	1.96	4.13	8.25	1.55
146	9.21	0.667	0.229	2.00	4.61	10.0	1.87
147	9.67	0.750	0.292	2.00	4.83	11.0	2.07
148	10.42	0.834	0.354	2.04	5.11	11.0	2.07
149	10.75	0.916	0.417	2.04	5.27	11.0	2.07
150	12.0	1.000	0.479	2.05	5.86	14.0	2.60
151	12.5	1.083	0.583	2.06	6.06	15.0	2.78
152	12.5	1.167	0.542	2.04	6.13	13.20	2.42
I153	11.50	1.167	0.500	1.92	5.99	13.0	2.40
154	10.38	1.083	0.437	1.90	5.46	10.5	1.97
155	10.17	1.000	0.375	1.88	5.41	11.0	2.07
156	9.50	0.916	0.375	1.86	5.10	10.0	1.87
157	9.00	0.834	0.354	1.86	4.89	9.5	1.78
158	8.33	0.750	0.250	1.86	4.48	8.67	1.63
159	7.54	0.667	0.250	1.85	4.08	8.0	1.50
160	7.21	0.583	0.250	1.84	3.92	8.50	1.60
161	6.75	0.500	0.250	1.84	3.68	13.0	2.20
162	6.00	0.417	0.146	1.84	3.26	7.0	1.32
163	5.42	0.333	0.167	1.83	2.96	9.3	1.73
164	4.92	0.250	0.104	1.84	2.67	7.0	1.32

Table 2. Dimensionless ratios computed from measured data, Runs 55-164, Sets A-I.

Run	Depth Diameter h/D	Height Diameter H/D	Fg ρD^5	Depth inches
A55	2.67	1.28	3370	12
56	2.45	1.22	3820	11
57	2.22	1.11	4940	10
58	2.00	0.78	3820	9
59	1.78	0.78	4720	8
60	1.55	0.88	3370	7
61	1.33	0.83	3370	6
62	1.11	0.39	2248	5
63	0.89	0.28	2470	4
64	0.67	0.22	2920	3
65	0.44	0.22	337	2
B66	0.44	0.26	337	2
67	0.67	0.26	674	3
68	0.89	0.33	1460	4
69	1.11	0.44	2470	5
70	1.33	0.50	2470	6
71	1.55	0.78	4270	7
72	1.78	0.67	4270	8
73	2.00	1.00	5840	9
74	2.22	1.06	5840	10
75	2.45	0.94	4940	11
76	2.67	0.94	4270	12
77	2.89	1.06	3820	13
78	3.11	1.11	3820	14
C79	3.11	1.06	4270	14
80	2.89	1.06	4270	13
81	2.67	1.17	4940	12
82	2.45	1.17	5390	11
83	2.22	0.94	4940	10
84	2.00	0.94	4940	9
85	1.78	0.89	4720	8
86	1.55	0.78	3600	7
87	1.33	0.50	2470	6
88	1.11	0.27	2020	5
89	0.89	0.33	2470	4
90	0.67	0.20	2470	3
91	0.44	0.20	898	2

Table 2. Dimensionless ratios computed from measured data, Runs 55-164, Sets A-I. (Continued)

Run	Depth Diameter h/D	Height Diameter H/D	Fg ρD^5	Depth inches
D92	0.67	0.16	3530	3
93	0.89	0.21	3710	4
94	1.11	0.33	2970	5
95	1.33	0.55	3370	6
96	1.55	0.55	4610	7
97	1.78	0.94	4650	8
98	2.00	0.89	4200	9
99	2.22	1.06	4990	10
100	2.45	1.33	5620	11
101	2.67	1.28	5840	12
102	2.89	1.39	4720	13
103	3.11	1.33	5400	14
E104	3.11	1.45	4990	14
105	2.89	1.17	4040	13
106	2.67	1.11	4380	12
107	2.45	1.06	4110	11
108	2.22	1.00	4110	10
109	2.00	0.78	3620	9
110	1.78	0.72	2920	8
111	1.55	0.67	3420	7
112	1.33	0.61	4950	6
113	1.11	0.50	3260	5
114	0.89	0.45	3030	4
115	0.67	0.33	2248	3
F116	0.44	0.17	1010	2
117	0.67	0.22	2700	3
118	0.89	0.28	2970	4
119	1.11	0.50	2970	5
120	1.33	0.55	4200	6
121	1.55	0.61	5400	7
122	1.78	0.78	6580	8
123	2.00	1.00	7050	9
124	2.22	1.06	6250	10
125	2.45	1.11	6070	11
126	2.67	1.22	5390	12
127	2.89	1.11	4950	13
128	3.11	1.11	4650	14

Table 2. Dimensionless ratios computed from measured data, Runs 55-164, Sets A-I. (Continued)

Run	Depth Diameter h/D	Height Diameter H/D	Fg ρD^5	Depth inches
G129	3.11	2.06	6250	14
130	2.89	1.33	4050	13
131	2.67	1.00	4200	12
132	2.45	1.00	4950	11
133	2.22	0.94	5390	10
134	2.00	0.83	4500	9
135	1.78	0.83	4270	8
136	1.55	0.61	4650	7
137	1.33	0.50	3420	6
138	1.11	0.22	2970	5
139	0.89	0.17	2490	4
140	0.67	0.17	1910	3
H141	0.67	0.17	2970	3
142	0.89	0.28	2490	4
143	1.11	0.33	2970	5
144	1.33	0.33	4610	6
145	1.55	0.45	3490	7
146	1.78	0.61	4200	8
147	2.00	0.78	4650	9
148	2.22	0.94	4650	10
149	2.45	1.11	4650	11
150	2.67	1.28	5840	12
151	2.89	1.55	6250	13
152	3.11	1.45	5440	14
I153	3.11	1.33	5440	14
154	2.89	1.17	4430	13
155	2.67	1.00	4650	12
156	2.45	1.00	4200	11
157	2.22	0.94	4000	10
158	2.00	0.67	3660	9
159	1.78	0.67	3370	8
160	1.55	0.67	3590	7
161	1.33	0.67	4940	6
162	1.11	0.39	2970	5
163	0.89	0.44	3880	4
164	0.67	0.28	2970	3

the family of curves for the force ratio of the different water depths from four inches to 14 inches.

From Figure 9, as the wave height increases, with constant depth, the force on the cylinder increases. Similarly, as the depth of water decreases, with constant wave height, the force exerted on the cylinder increases. The change in the latter case is smaller than for increasing wave height.

As the depth of water increases, the slopes of the curves decrease. This indicates that the effect of increasing the wave height a given amount at a small depth is greater than the effect of the same increase at a greater depth.

Two wave cycles of each run of Set E are presented in Figure 10. The waves generated varied considerably from smooth, sinusoidal shapes. The deeper water produced smoother traces as the waves were less affected by the cylinder and the bottom. This series of runs started with deep water (Run 104) and decreased to the three-inch depth (Run 115). When the water depth decreased to eight inches, a tendency for the wave to spill over the four and one-half inch cylinder was noted. See Photographs 2, 3, and 4. Reflection of the wave was first noticed at the six-inch depth. The slight positive slope in each trace occurred due to a small preceding wave developed by the wave generator. This small wave was visually observed in nearly all the runs. The waves produced remained periodic over a period of ten minutes. No length or force characteristic changed appreciably.

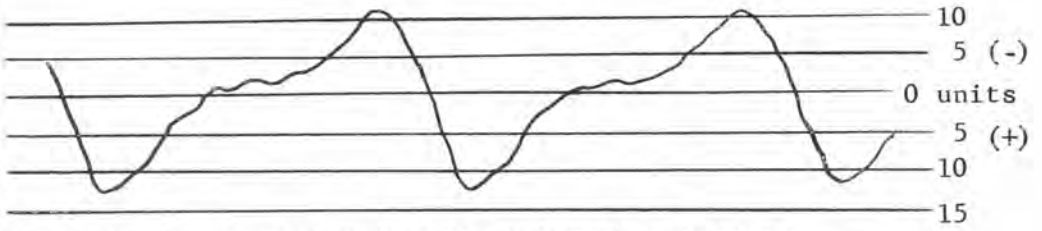

Run 104. WL=11.75', h=1.167', H=0.542', F=2.22 lb.

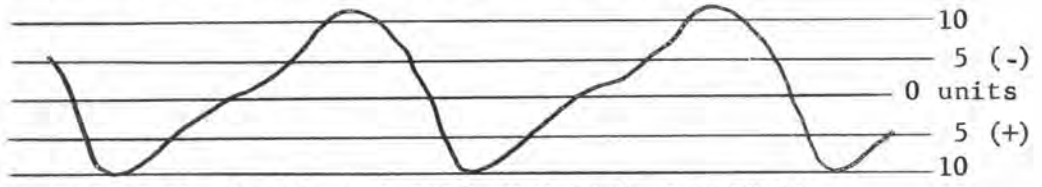

Run 105. WL=10.75', h=1.083', H=0.437', F=1.80 lb.

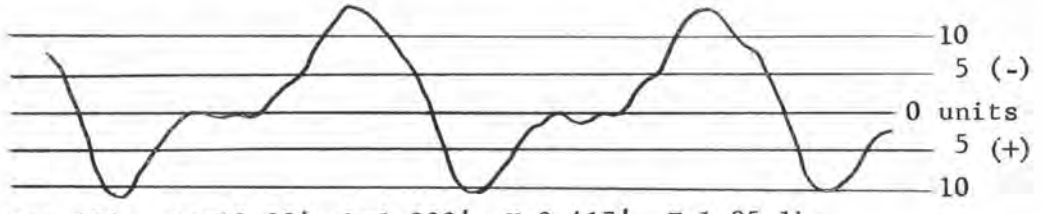

Run 106. WL=10.29', h=1.000', H=0.417', F=1.95 lb.

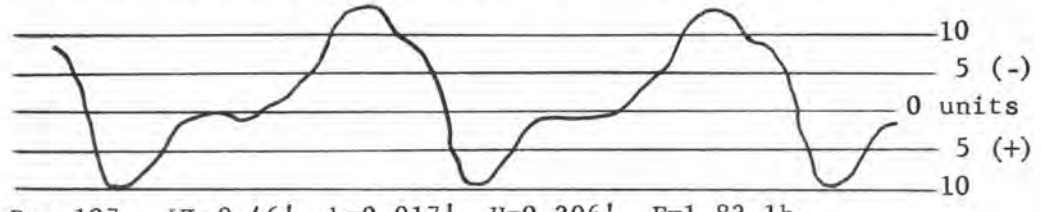

Run 107. WL=9.46', h=0.917', H=0.396', F=1.83 lb.

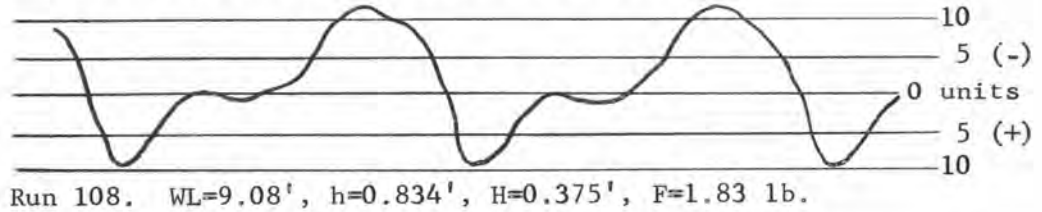

Run 108. WL=9.08', h=0.834', H=0.375', F=1.83 lb.

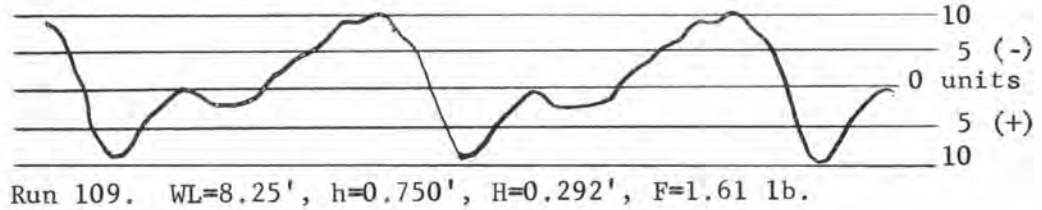

Run 109. WL=8.25', h=0.750', H=0.292', F=1.61 lb.

Figure 10. Variability of measured force during a wave cycle. Period = 1.86 seconds. Runs 104-115.

Run 110. WL=7.50', h=0.667', H=0.271', F=1.30 lb.

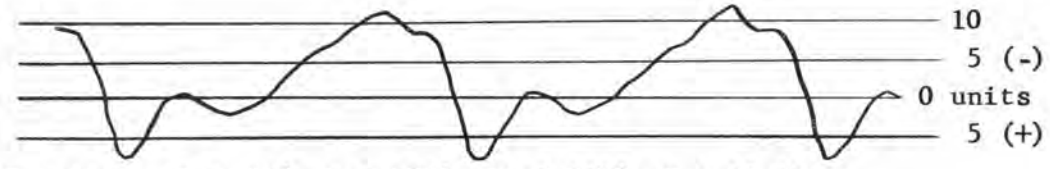

Run 111. WL=6.96', h=0.583', 11=0.250', F=1.52 lb.

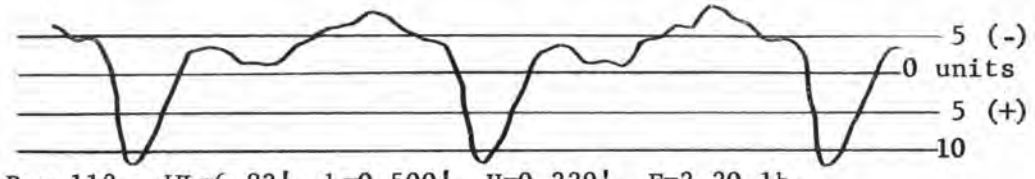

Run 112. WL=6.83', h=0.500', H=0.229', F=2.20 lb.

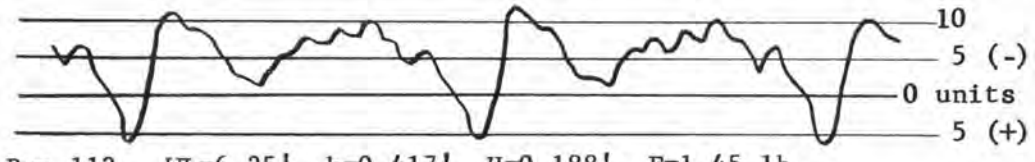

Run 113. WL=6.25', h=0.417', H=0.188', F=1.45 lb.

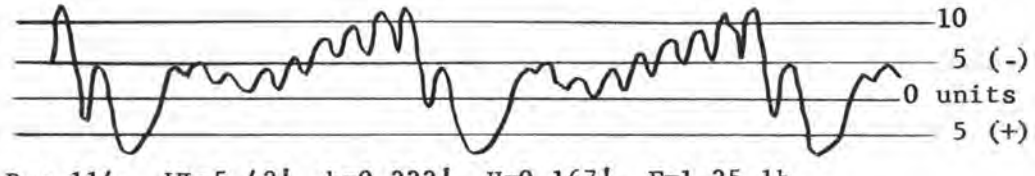

Run 114. WL=5.42', h=0.333', H=0.167', F=1.35 lb.

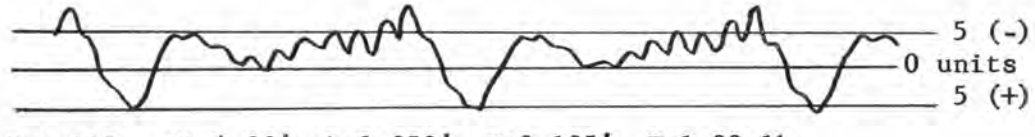

Run 115. WL=4.92', h=0.250', H=0.125', F=1.00 lb.

Figure 10. Variability of measured force during a wave cycle. Period = 1.86 seconds. Runs 104-115. (Cont.)

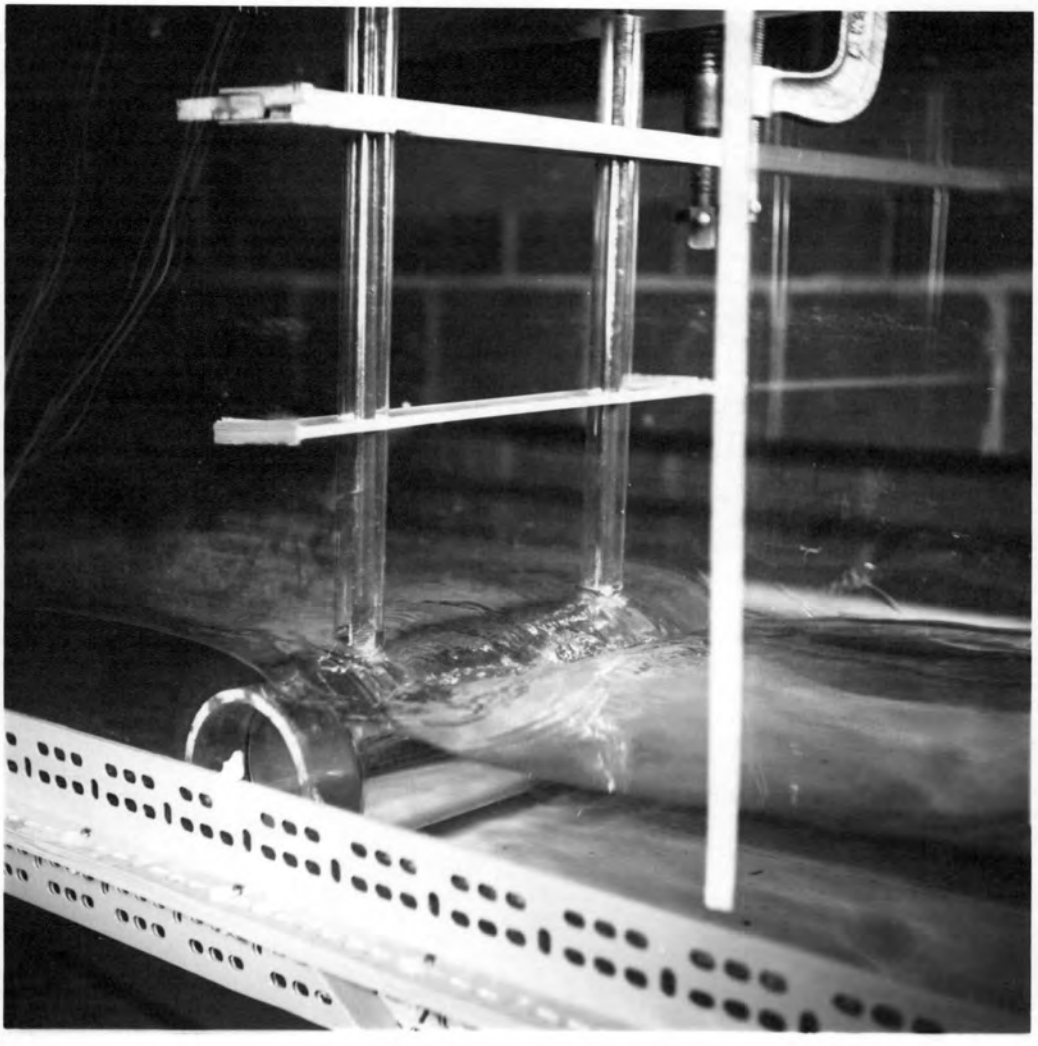

Photograph 3. Wave backwash. Still water depth = 6 inches. Direction of wave propagation from right to left.

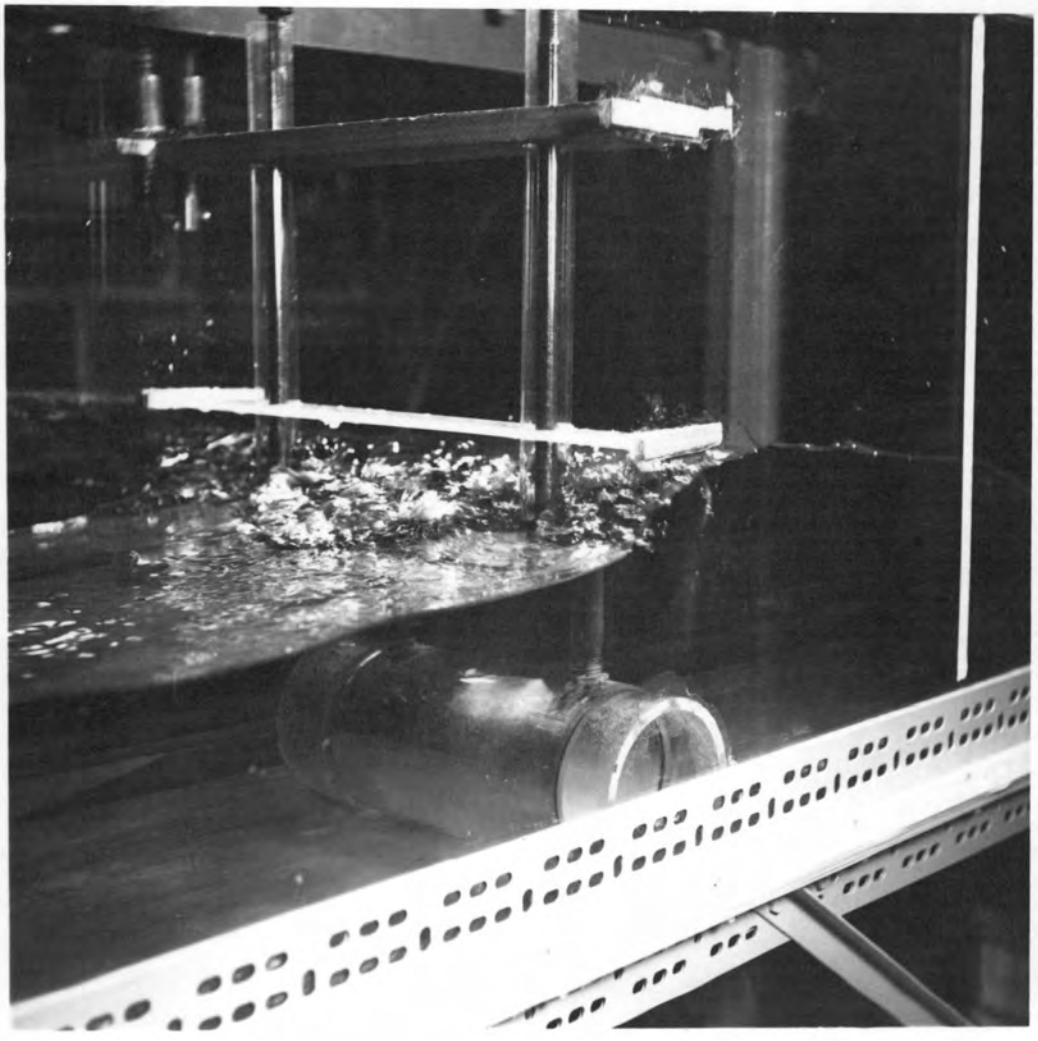

Photograph 4. Shoaling effect. Still water depth = 8 inches. Direction of wave propagation from right to left.

Comparison of Pressure Forces

The theoretical oscillatory pressure distribution, Equation (28), was integrated graphically to give the potential flow pressure forces affecting a four and one-half inch cylinder. The pressure forces obtained are maximum values, occurring once every complete wave cycle (See Table 3). The horizontal pressure force is compared with the measured maximum force given in Table 1. The same wave characteristics were used in the computer solution to determine the pressure distribution as was measured in the wave tank.

Table 3 indicates, with one exception, that the percentage difference between the computed horizontal force and the measured drag increases as the depth of water decreases. Further reconciliation of the difference between the computed and measured forces must come from consideration of viscous and inertial effects, which were neglected in the derivation of the pressure distribution (Equation (28)). Runs 104 through 115, considered a representative set, were used for graphical integration computation and presented in Table 3. From this data the inertial and viscous effects appear to increase as the depth decreases, indicating that the flow is increasingly turbulent. Potential flow exists to a greater extent with increased depths.

Runs conducted with five-inch depths (Run 113) exposed the cylinder when the trough of the wave went by. A water depth of five inches was the limiting value for computer solution as the cylinder diameter is four and one-half inches. For lower water depths the wave particle

Table 3. Comparison of measured and theoretical pressure forces.

Run	Depth inches	Computed Horizontal Force - lb.	Measured Drag lb.	Percent Difference	Computed Lift lb.
E104	14	1.55	2.22	30.2	8.42
105	13	1.51	1.80	16.1	8.25
106	12	1.47	1.95	24.6	8.37
107	11	1.38	1.83	24.6	8.12
108	10	1.34	1.83	26.7	7.73
109	9	1.08	1.61	32.9	7.03
110	8	0.73	1.30	43.8	7.08
111	7	0.69	1.52	54.6	7.17
112	6	0.65	2.20	70.8	7.51
113	5	0.48	1.45	66.9	7.55
114	4	--	1.35	---	--
115	3	--	1.00	--	--

motion over the cylinder does not approach potential flow motion and the large error results.

Particle motion (Equation (25)) decreases as the depth increases, with a constant wave height. Also, particle motion increases with increasing wave height, depth remaining constant. Because of the nature of the waves generated, the height of the waves in the wave tank increased as the depth of water increased. This increased wave height offset the depth increase with resultant particle motion actually increasing. As shown in Table 1 and Table 3, the forces increased with increasing depth. The computed horizontal pressure force can still be compared to the measured drag because the same characteristic wave dimensions were also used in determining the pressure distribution.

Beckmann and Thibodeaux (See Page 8) give the range that can be expected in the drag and lift coefficients for cylinders in contact with a flat boundary. Their expected range for the coefficient of drag is $0.35 \leq C_D \leq 0.40$ and for the lift coefficient to be: $0.34 \leq C_L \leq 0.65$. Table 4 presents the measured C_D using the maximum force (Table 1) and the wave velocity for Set E, Runs 104 through 115. The measured C_D closely agreed with that given by Beckmann and Thibodeaux for shallow depths but was one-half their value at the higher depths. C_D and C_L for the graphical integration case are included for academic interest as the viscous and inertial effects are absent.

Table 4. Comparison of measured and theoretical drag and uplift coefficients.

Run	Depth (inches)	Measured C_D (Max. force)	Graphical Integration C_D (Max. force)	Graphical Integration C_L (Max. uplift)
E104	14	0.16	0.12	0.61
105	13	0.15	0.13	0.71
106	12	0.18	0.13	0.77
107	11	0.20	0.15	0.88
108	10	0.21	0.16	0.91
109	9	0.22	0.15	0.98
110	8	0.23	0.13	1.22
111	7	0.29	0.13	1.37
112	6	0.44	0.13	1.50
113	5	0.35	0.12	1.80
114	4	0.43	--	--
115	3	0.37	--	--

Added Mass Effect of Cylinder

The force measurements taken depended entirely upon a slight deflection of the test cylinder, which actuated the strain gages. The maximum deflections obtained were approximately one-quarter of an inch. With this large deflection, the added mass effect discussed previously was investigated briefly. The mass of the deflecting cylinder was increased by the addition of water inside the cylinder. No noticeable change occurred in any of the wave or force characteristics obtained from the oscillograph trace as a result of increasing the mass of the cylinder.

CONCLUSIONS AND RECOMMENDATIONS

Generally, the force on the cylinder decreases with increasing depth, with constant wave height. The force on the cylinder increases with increasing wave height, with constant depth. The writer believes the data scatter present is primarily from the visual recording of wave height and water depth, with some data scatter from the irregular shape of the wave. Instrumentation to provide accurately recorded measurement of the wave characteristics is desired.

The writer considers the wave height to be an important variable in determining the horizontal force on the cylinder. A slight variation in height, for a given depth, will increase the force ratio $F_g/\rho D^3$ an even greater amount. Any observational error in the measurement of the wave height will thus be magnified when the height ratio H/D is plotted against the force ratio.

The large differences between the computed horizontal pressure force and the measured drag were expected at the shallower depths due to increasing viscous and inertial effects. The difference being less with increased depth indicates the flow pattern over the cylinder to approach potential flow theory. The pressure distribution equation derived is usable when the depth ratio, h/D, is greater than three.

The coefficient of drag, C_D, computed from the measured force agrees closely at the shallower depths with the C_D range given by Beckmann and Thibodeaux as $0.35 \leq C_D \leq 0.40$. With depths greater than seven inches, the measured C_D decreased to approximately one-half

the value given by Beckmann and Thibodeaux. The wave velocity squared becomes larger as the depths increase, this could account for the decreased value of C_D.

The value of C_D obtained by graphical integration of the pressure distribution agrees well with the measured C_D at depths above ten inches. This indicates the effects of inertia and viscosity are of increasing importance at the shallower depths, where the turbulence is greatest.

Further investigations should include the experimental measurement of the pressure distribution using a rapid sampling pressure scanner and transducer. Experimental pressure distributions should be integrated to determine the horizontal force and the uplift, for comparison with the theoretical pressure distribution equation.

The attempt made to determine the uplift from the test cylinder deflection yielded inconclusive results. Further investigations should determine cylinder uplift by allowing cylinder movement only in the vertical plane.

BIBLIOGRAPHY

1. Airy, G. B. On tides and waves. In: Encyclopaedia Metropolitana, vol. 5, London, 1845. (Cited in Transactions, ASCE, Paper No. 3182, 1962. p. 668).

2. Alterman, I. Submarine outfall pipe for the disposal of sewage and industrial wastes. Haifa, Israel, 1958. 64 numb. leaves. (Technion - Israel Institute of Technology, Division of Hydraulic Engineering).

3. Alterman, I. Discussion. Wave force coefficients for offshore pipelines. Journal of the Waterways and Harbors Division, Proceedings of the American Society of Civil Engineers 88(WW4):149-150. 1962.

4. Beckmann, Herbert and Murphy H. Thibodeaux. Wave force coefficients for offshore pipelines. Journal of the Waterways and Harbors Division, Proceedings of the American Society of Civil Engineers 88(WW2):125-138. 1962. (Proceedings Paper No. 3141).

5. Collins, S. V. S. Submersible pipelines round the world. Surveyor 119(3577):1449-1453. December 24, 1960.

6. Crooke, R. Curtis. Re-analysis of existing wave force data on model piles. Temple City, California, 1955. 22 numb. leaves. (Beach Erosion Board.Technical Memorandum No. 71, April, 1955).

7. Dean, Robert G. et al. Estuary and coastline hydrodynamics. Cambridge, 1960. 266 numb. leaves. (Massachusetts Institute of Technology, Department of Civil and Sanitary Engineering, Hydrodynamics Laboratory).

8. Iversen, H. W. and R. Balent. A correlating modulus for fluid resistance in accelerated motion. Journal of Applied Physics 22 (3):324-328. 1951.

9. Keim, S. Russell. Fluid resistance to cylinders in accelerated motion. Journal of the Hydraulics Division, Proceedings of the American Society of Civil Engineers 82(HY6):1113-1 - 1113-14. 1956. (Proceedings Paper No. 1113).

10. Keulegan, Garbis H. and Lloyd H. Carpenter. Forces on cylinders and plates in an oscillating fluid. Journal of Research of the National Bureau of Standards 60(5):423-440. 1958. (Research Paper No. 2857).

11. Laird, A. D. K. and C. A. Johnson. Drag forces on an accelerated cylinder. Journal of Petroleum Technology, AIMME, 8(5):65-67, 1956. (Technical Note No. 338).

12. McNown, John S. Drag in unsteady flow. In: Proceedings of the 9th International Congress for Applied Mechanics, Brussells, 1956, vol. 3. Brussells University, 1957. p. 124-134.

13. McNown, John S. and G. H. Keulegan. Vortex formation and resistance in periodic motion. Journal of the Engineering Mechanics Division, Proceedings of the American Society of Civil Engineers 85(EM1):1-6. 1959. (Proceedings Paper No. 1894).

14. Milne-Thomson, L. M. Theoretical hydrodynamics. 4th ed. New York, MacMillan, 1960. 660 p.

15. Rayleigh, Lord. On the motion of solid bodies through viscous liquid. Philosophical Magazine and Journal of Science, Series Six, 21(126):697-711. 1911. (Paper No. LXXXII).

16. Russell, R. C. H. and D. H. MacMillan. Waves and tides. London, Hutchinson's Scientific and Technical Publications, 1952. 348 p.

17. Ryan, William Lee. Characteristics of jet diffusers for ocean outfalls. Master's thesis. Corvallis, Oregon State University, 1962. 63 numb. leaves.

18. Schlichting, Hermann. Boundary layer theory. 4th ed. New York, McGraw-Hill, 1960. 647 p.

19. Shames, Irving H. Mechanics of fluids. New York, McGraw-Hill, 1962. 555 p.

20. Stelson, Thomas E. and Frederic T. Mavis. Virtual mass and acceleration in fluids. Transactions of the American Society of Civil Engineers 122:518-530. 1957. (Paper No. 2870).

21. Stokes, G. G. On the theory of oscillating waves. In: G. G. Stokes' Mathematical and Physical Papers, vol. 1, Cambridge, Cambridge University Press, 1880. p. 197-229. (From the Transactions of the Cambridge Philosophical Society, 8:441+).

22. Vallentine, H. R. Applied hydrodynamics. London, Butterworths, 1959. 272 p.

APPENDICES

APPENDIX I

IBM FORTRAN Computer Solution
Pressure Distribution Equation

IBM FORTRAN COMPUTER SOLUTION

PRESSURE DISTRIBUTION EQUATION

The equation for the pressure distribution around a circular cylinder resting on a flat boundary in an oscillating fluid was derived (Equation (28)) to be:

$$P = \gamma\left[d - y_c + \frac{H}{2}\sin 2\pi\left(\frac{x}{L} - \frac{t}{T}\right)\right]$$

$$+\left[\frac{\rho\pi^2H^2}{2T^2\sinh^2(2\pi d/L)}\right]\left[\cosh^2 2\pi(d+z_y)/L\right] \qquad (28)$$

$$\left[\cos^2 2\pi\left(\frac{x}{L} - \frac{t}{T}\right)\right]\left[1 - \frac{a^2\pi^4}{4(y_c)^2\cosh^4(a\pi x/r^2)}\right].$$

In this computer solution, all of the terms will be placed in floating point notation, as indicated in Table 5.

Table 5. Symbols in text's equations condensed for computer programming.

Equation	Program	Definition
a	RAD	Radius of cylinder.
d	D	Depth to still water surface.
H	H	Height of wave.
L	WL	Wave length.
r^2	R2	Chord length = 2(a)(Yc).
t	TX	Fraction of wave period.
T	TT	Wave period.
x	X	Horizontal cylinder and wave coordinate.
Yc	YC	Vertical cylinder coordinate.
Zy	ZY	Vertical distance from still water surface to cylinder.
γ	SPWT	Specific weight of the fluid.
π	PI	3.1415927.
ρ	RHO	Mass density of the fluid.

In simplifying the computer solution, several of the above terms combine into single terms involving two like letters. This was done to facilitate the computer solution and flow chart analysis. Table 6 gives the combined terms. Figure 12 gives the flow chart solution, followed by the computer program.

Table 6. Condensed computer program symbols.

Symbol	Expanded
CC	$2\pi d/L$.
DD	$a\pi X/r^2$.
EE	$2\pi(X/L - t/T)$.
FF	$2\pi(d + Zy)/L$.
PP	$\text{Sinh}^2(CC)$.
AA	$\rho\pi^2 H^2/2T^2(PP)$.
QQ	$\cosh^4(DD)$.
BB	$1 - a^2\pi^4/4(YC)^2(QQ)$.
HH	$\cosh^2(FF)$.
GG	$\cos^2(EE)$.
UU	(AA)(GG)(HH).
ZY	-D + Yc.
PO	$\gamma[d - Yc + H \sin(EE)/2]$.
P	Pressure, lbs. per ft.^{2}

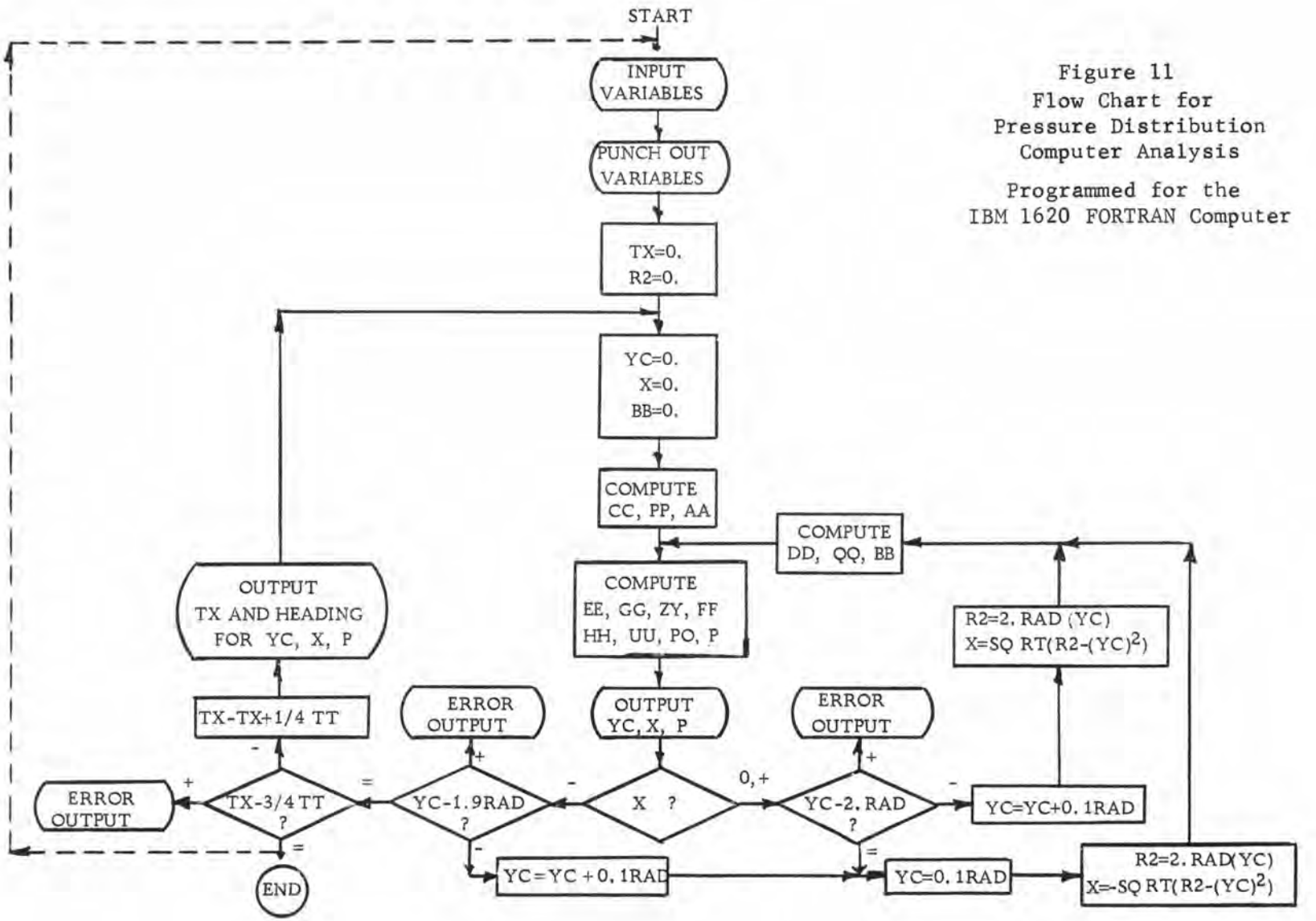

Figure 11
Flow Chart for
Pressure Distribution
Computer Analysis

Programmed for the
IBM 1620 FORTRAN Computer

IBM 1620 FORTRAN COMPUTER SOLUTION, PRESSURE DISTRIBUTION

```
  3 READ33,RAD,D,H,WL,TT,RHO,SPWT
 33 FORMAT(F5.3,F6.3,F5.3,F6.2,F4.2,F4.3,F4.2)
    PUNCH 9
  9 FORMAT(9HVARIABLES/)
    PUNCH 5
  5 FORMAT(47H  RAD      D      H      WL     TT    RHO    SPWT)
    PUNCH4,RAD,D,H,WL,TT,RHO,SPWT
  4 FORMAT(F7.3,F8.3,F7.3,F8.2,F6.2,F6.3,F6.2/)
    PI=3.1415927
    TX=0.
    R2=0.
  6 YC=0.
    X=0.
    PUNCH 26,TX
 26 FORMAT(/34H THE FRACTION OF THE WAVE PERIOD IS,F6.2,1X,4HSEC./).
    PUNCH 10
 10 FORMAT(26H    YC      X     PRESS(PSI)/)
    BB=1.
    CC=(2.*PI*D)/WL
    PP=((EXP(CC)-1./ESP(CC))/2.)**2
    AA=(.5*RHO*PI*H*H)/(TT*TT*PP)
    GO TO 8
  7 DD=(RAD*PI*X)/R2
    QQ=((EXP(DD)+1./EXP(DD))/2.)**4
    BB=1.-RAD*RAD*PI**4/(4.*YC*YC*QQ)
  8 EE=2.*PI*(X/WL-TX/TT)
    GG=COS(EE)*COS(EE)
    ZY=-(D-YC)
    FF=2.*PI*(D+ZY)/WL
    HH=((EXP(FF)+1./EXP(FF))/2.)**2
    UU=AA*HH*GG
    PO=SPWT*(D-YC+(H*SIN(EE))/2.)
    P=(PO+UU*BB)/144.
    PUNCH 11,YC,XP
 11 FORMAT(F8.3,F7.3,E11.5)
    IF(X)13,12,12
 13 IF(YC-1.9*RAD)14,15,16
 16 PRINT 17
 17 FORMAT(31HERROR,YC GREATER THAN ALLOWABLE)
 14 YC=YC+(.1*RAD)
    GO TO 21
 12 IF(YC-2.*RAD)18,19,20
 20 PUNCH 17
 18 YC=YC+(.1*RAD)
    X=SQRT(2.*RAD*YC-YC*YC)
```

IBM 1620 FORTRAN COMPUTER SOLUTION, PRESSURE DISTRIBUTION Cont.

```
   R2=2.*RAD*YC
   GO TO 7
19 YC=.1*RAD
21 X=-SQRT(2.*RAD*YC-YC*YC)
   R2=2.*RAD*YC
   GO TO 7
15 IF(TX-(.75*TT))22,23,24
24 PUNCH 25
25 FORMAT(24HERROR,TX GREATER THAN TT)
22 TX=TX+TT/4.
   GO TO 6
23 PAUSE
   GO TO 3

   END
```

APPENDIX II

Comparison of Steady and Unsteady Pressure Distributions

COMPARISON OF STEADY AND UNSTEADY PRESSURE DISTRIBUTIONS

The steady flow solution cannot be compared identically with the unsteady pressure distribution due to the very nature of the problem. The steady flow solution has constant particle velocity, which, for the comparison cited here, will be equivalent to the maximum horizontal particle velocity of the unsteady case, and is everywhere constant. The particle velocity for the unsteady case, however, not only varies spatially but is dependent on time in a prescribed oscillatory manner. Thus, the absolute magnitudes of the two solutions cannot be compared; rather, the pressure about the cylinder in a steady flow condition will be related to the unsteady flow case by varying the time period and noting relative magnitude changes of the two solutions.

The constants used are from run number 12:

Radius	= 0.188 feet
Depth	= 0.500 feet
Wave height	= 0.333 feet
Wave length	= 8.67 feet
Period of wave	= 2.10 seconds
Density	= 1.940 lb. sec^2/ft^4
Specific weight	= 62.40 lb/ft^3
Velocity (steady flow case)	= 1.55 ft/second

The velocity was computed from Equation (24) as

$$U_x = \pi H \cosh\left[2\pi(d+z_y)/L\right] \cos\left[2\pi\left(\frac{x}{L}-\frac{t}{T}\right)\right]$$

$$= \frac{(3.14)(0.333)}{2.10} \coth\left[\frac{(6.28)(0.500)}{(8.67)}\right]$$

$$= 1.42 \text{ ft/sec.}$$

Table 7 presents the steady flow pressure distribution as obtained from Equation (19), remembering that P_o depends on the level under consideration (See Figure 12):

$$P = P_o + \frac{\rho U^2}{2}\left[1 - \frac{a^2\pi^4}{4(y_c)^2\cosh^4(a\pi x/r^2)}\right]. \quad (19)$$

Table 7. Theoretical steady flow pressure distribution data about a cylinder.

Point	YC, ft.	X, ft.	Pressure lb/ft.	Pressure lb/in.
1	0.000	0.000	33.2	0.231
2	0.018	0.018	32.1	0.223
3	0.056	0.134	29.7	0.206
4	0.112	0.172	26.0	0.181
5	0.188	0.188	20.2	0.140
6	0.244	0.179	14.8	0.103
7	0.300	0.150	8.3	0.0576
8	0.338	0.122	4.0	0.0278
9	0.357	0.081	0.4	0.0028
10	0.376	0.000	-2.3	-0.0160
11	0.018	-0.081	32.1	0.223
12	0.056	-0.134	29.7	0.206
13	0.112	-0.172	26.0	0.181
14	0.188	-0.188	20.2	0.140
15	0.244	-0.179	14.8	0.103
16	0.300	-0.150	8.3	0.0576
17	0.338	-0.122	4.0	0.0278
18	0.357	-0.081	0.4	0.0028

The unsteady, or oscillatory, pressure distribution data was obtained from the computer solution described in Appendix I. The computer solution was designed to give points about the cylinder at one-quarter wave period intervals. Representative points are given in Table 8 and are shown with the wave profile in Figures 13, 14, 15, and 16.

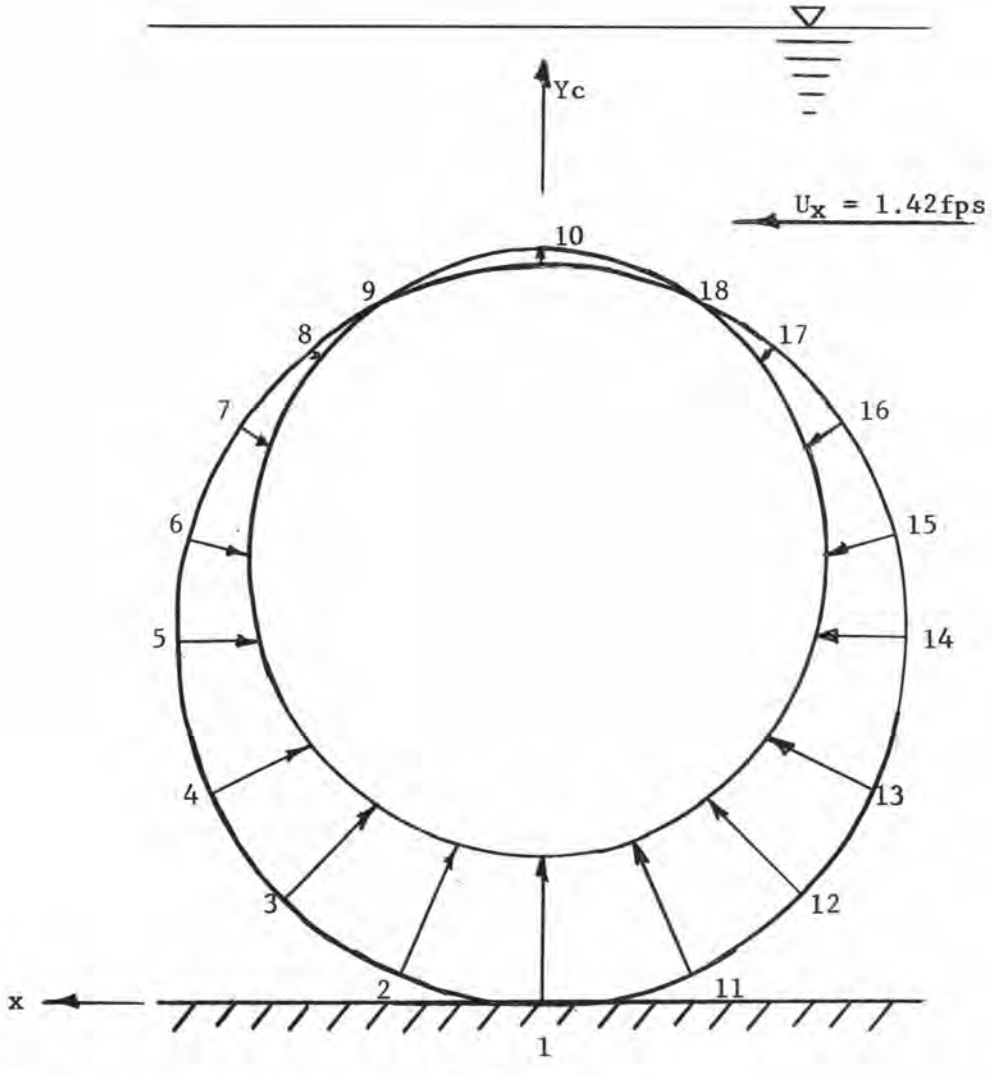

Note: Length scale: 1in. = 0.1 ft.
Pressure scale: 1in. = 0.300 psi.
Positive pressure measured inward.

Figure 12. Steady flow pressure distribution about a cylinder. Data from Run 12.

Table 8. Theoretical unsteady flow pressure distribution data about a cylinder.

Point	Yc, ft.	x, ft.	Pressure Period = 0.00 sec lb./ft.^{2}	lb./in.^{2}	Pressure Period = 0.52 sec lb./ft.^{2}	lb./in.^{2}	Pressure Period = 1.05 sec lb./ft.^{2}	lb./in.^{2}	Pressure Period = 1.57 sec lb./ft.^{2}	lb./in.^{2}
1	0.000	0.000	32.9	0.229	20.8	0.145	32.9	0.229	41.6	0.289
2	0.018	0.081	31.1	0.216	19.7	0.137	32.4	0.225	40.4	0.281
3	0.056	0.134	28.4	0.197	17.4	0.120	30.4	0.211	38.1	0.264
4	0.112	0.172	24.5	0.170	13.9	0.096	27.1	0.188	34.5	0.240
5	0.188	0.188	18.7	0.130	9.2	0.064	21.5	0.150	29.8	0.207
6	0.244	0.179	13.6	0.094	5.6	0.039	16.3	0.113	26.2	0.182
7	0.300	0.150	7.5	0.052	2.1	0.014	9.8	0.068	22.7	0.158
8	0.338	0.112	2.9	0.020	- 0.3	-0.002	4.6	0.032	20.4	0.142
9	0.357	0.081	0.4	0.003	- 1.5	-0.010	1.6	0.011	19.3	0.134
10	0.376	0.000	- 1.9	-0.013	- 2.7	-0.018	31.2	0.216	18.1	0.126
11	0.018	-0.081	32.4	0.225	19.7	0.137	28.4	0.197	40.4	0.281
12	0.056	-0.134	30.4	0.211	17.4	0.120	24.5	0.170	38.1	0.264
13	0.112	-0.172	27.1	0.188	13.9	0.096	18.7	0.130	34.5	0.240
14	0.188	-0.188	21.5	0.150	9.2	0.064	13.6	0.094	29.8	0.207
15	0.244	-0.179	16.3	0.113	5.6	0.039	7.5	0.052	26.2	0.182
16	0.300	-0.150	9.8	0.068	2.1	0.014	2.9	0.020	22.7	0.158
17	0.338	-0.112	4.6	0.032	- 0.3	-0.002	0.4	0.003	20.4	0.142
18	0.357	-0.081	1.6	0.011	- 1.5	-0.010	-1.9	-0.013	19.3	0.134

The wave period, T, is 2.10 seconds, wave length = 8.67 ft., depth = 0.500 ft, and wave height = 0.333 ft. Data from Run number 12.

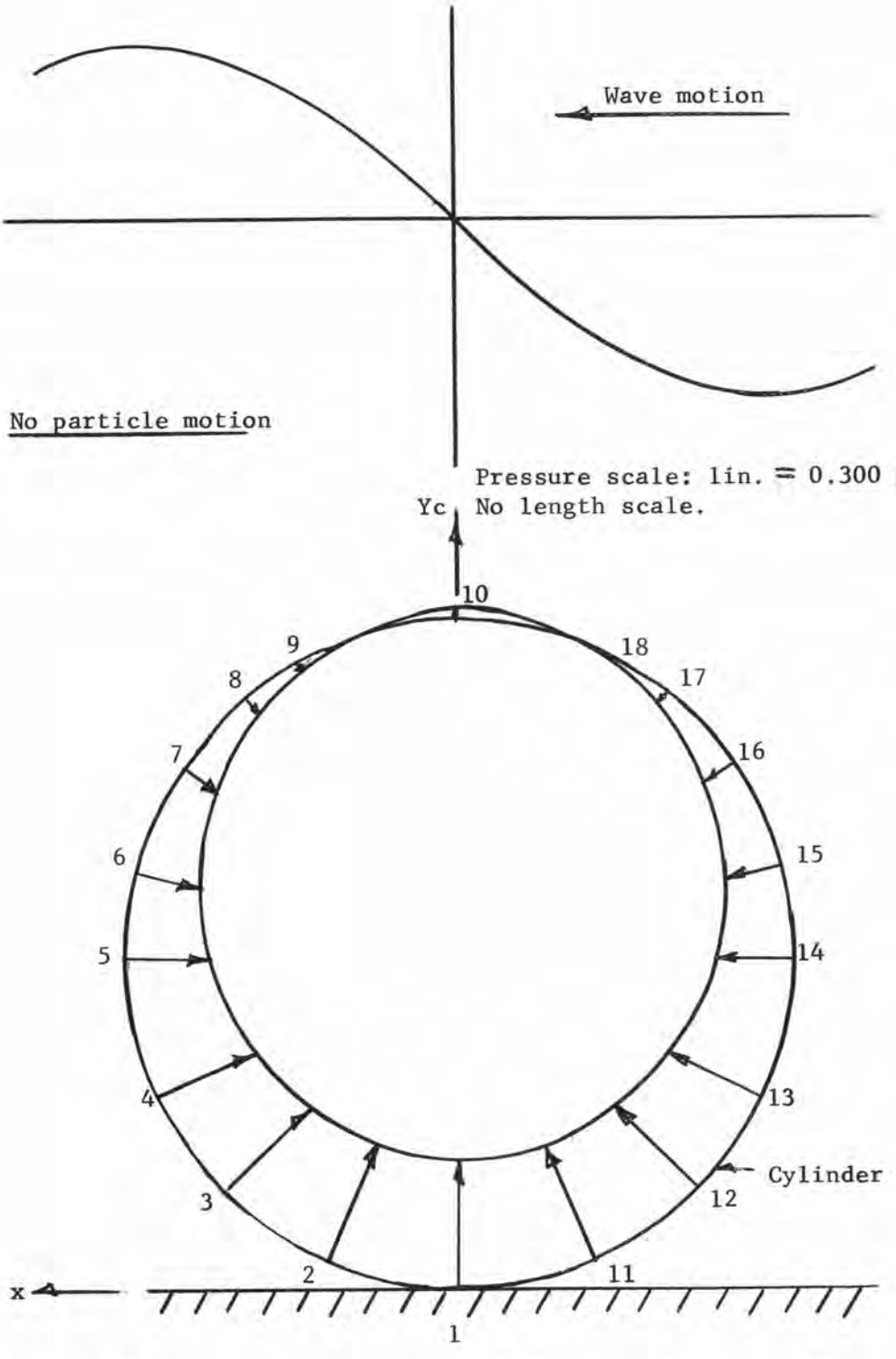

Figure 13. Unsteady pressure distribution, about a cylinder, fraction of wave period = 0.0 seconds (tx = 0.0).

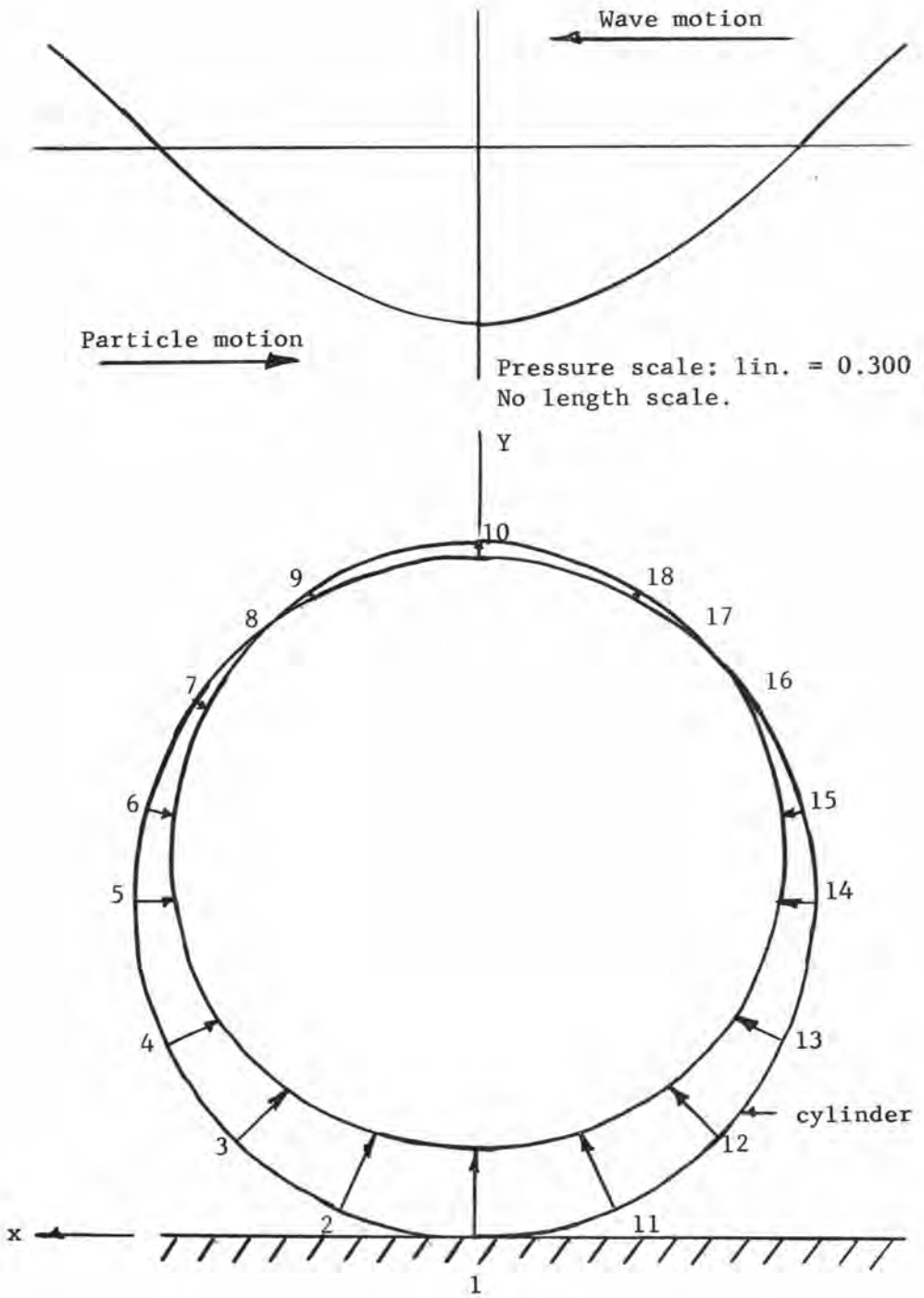

Figure 14. Unsteady pressure distribution about a cylinder, fraction of wave period = 0.52 seconds (tx = 1/4TT).

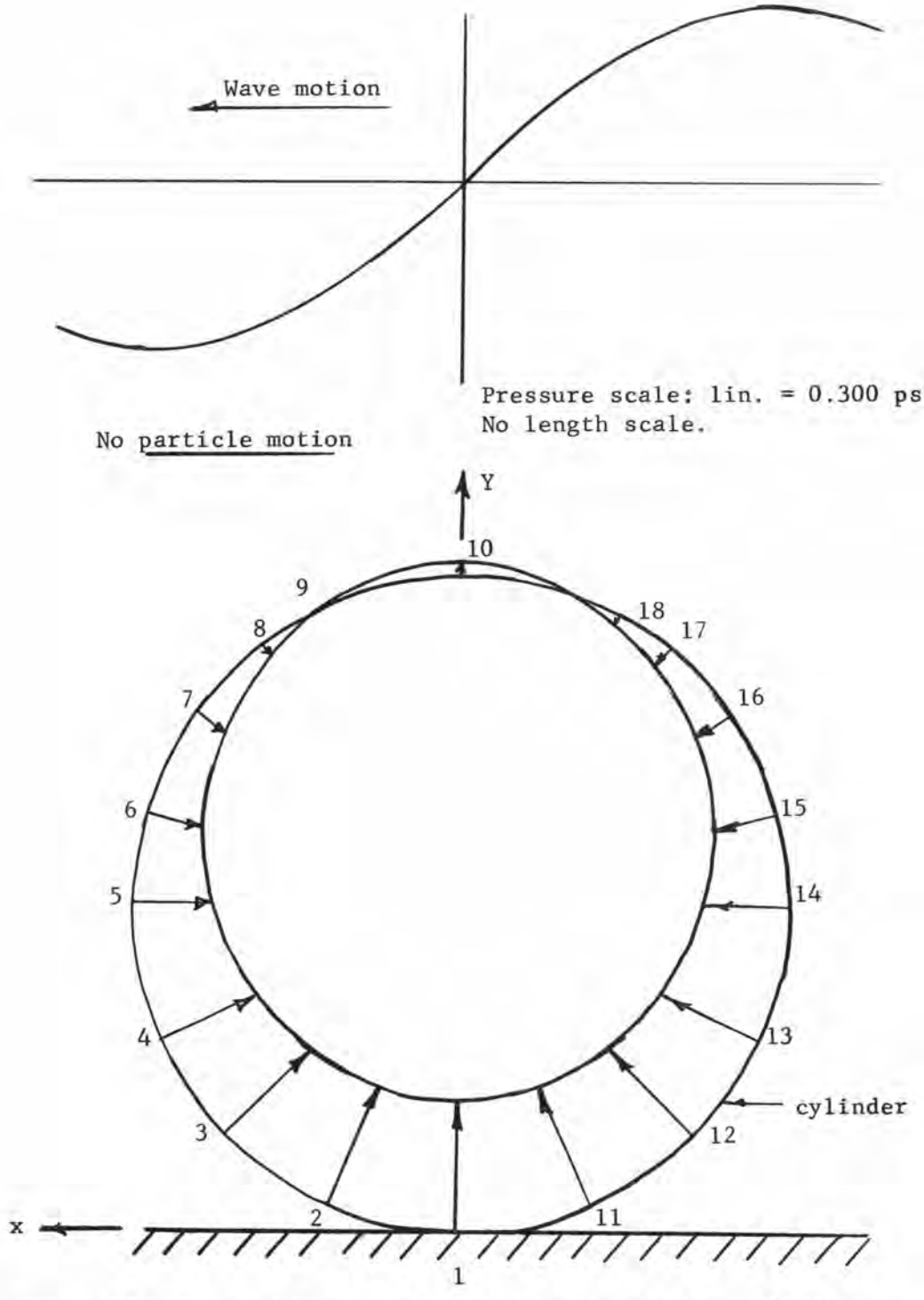

Figure 15. Unsteady pressure distribution about a cylinder, fraction of wave period = 1.05 seconds(tx = 1/2 TT).

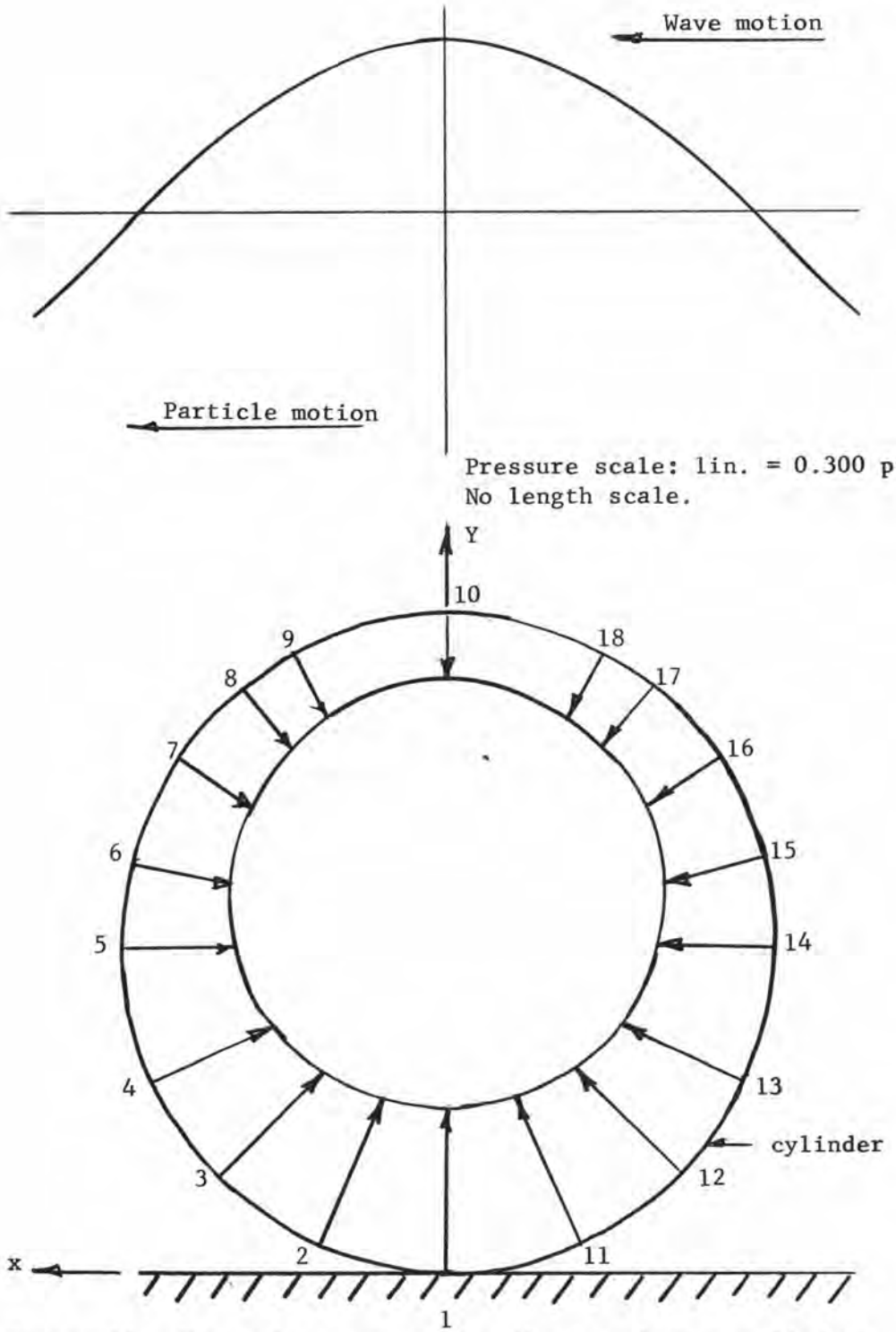

Figure 16. Unsteady pressure distribution about a cylinder, fraction of wave period = 1.57 seconds (tx = 3/4 TT).